PHOTOEMISSION STUDIES OF CLEAN AND ADSORBATE COVERED METAL SURFACES USING SYNCHROTRON AND UV RADIATION SOURCES

Gustav Richard Apai II

(Ph.D. Thesis)

PHOTOEMISSION STUDIES OF CLEAN AND ADSORBATE COVERED METAL SURFACES USING SYNCHROTRON AND UV RADIATION SOURCES

Contents

PHOTOEMISSION STUDIES OF CLEAN AND ADSORBATE COVERED METAL SURFACES USING SYNCHROTRON AND UV RADIATION SOURCES

Gustav Richard Apai II

Materials and Molecular Research Division
Lawrence Berkeley Laboratory
and
Department of Chemistry
University of California
Berkeley, California 94720

ABSTRACT

Photoemission energy distribution experiments on clean metal and adsorbate covered surfaces are performed under ultra-high vacuum conditions using x-ray and ultraviolet photon sources in the laboratory as well as continuously-tunable, highly polarized synchrotron radiation obtainable at the Stanford Synchrotron Radiation Laboratory (SSRL).

Studies are focused on two general areas:

1) Cross-section modulation in the photoemission process has been studied as a function of photon energy and orbital composition. Sharp decreases in intensity of the valence bands of several transition metals (i.e., Ag, Au, and Pt) are attributed to the radial nodes in the respective wavefunctions.

2) Adsorbate photoemission studies of CO adsorbed on platinum single crystals have demonstrated a very high spectral sensitivity to the 4σ and $(1\pi + 5\sigma)$ peaks of CO at photon energies of 150 eV. Angle-resolved photoemission has allowed us to determine the orientation of CO chemisorbed on a Pt(111) or Ni(111) surface. Preliminary results at high photon energies

(~150 eV) indicate scattering from the substrate which could yield chemisorption site geometries.

INTRODUCTION

Photoelectron Spectroscopy (PES) measures the kinetic energy distribution of photoemitted electrons from a given sample. For a fixed photon energy the photoemitted electron energy distribution reveals the energy and relative population of the allowed ionic states of the system. In atomic and molecular PES the final continuum states are relatively structureless, and the spectra can be rather straightforwardly interpreted in terms of the ground state electronic structure of the atom or molecule. For solids, however, the lattice periodicity imposes discrete structure on the "free" electron final states. The result is that the photoemission energy distribution which is obtained by exciting valence electrons in solids depends mainly on three quantities: the initial density of states, the final density of states, and the photoexcitation matrix element. The latter two define the photoemission cross-section. In ultraviolet photoemission spectroscopy (UPS), variations with photon energy in the photoelectron energy distribution obtained by exciting valence electrons are usually discussed in terms of final state effects which are responsible for the observed line positions and transition matrix element modulations which determine line intensities.[1] These we have called "band-structure-type" effects. Above the ultraviolet (UV) regime ($\hbar\omega > 80$ eV) additional "atomic-type" cross-section modulations may influence the photoelectron energy distribution. A tunable light source is required to determine this contribution to the photoemission spectrum. One

principal task of this thesis is to describe the "atomic-type" effect and illustrate its importance as it applies to the study of substrate-adsorbate systems. Chapter I discusses some of the characteristics of synchrotron radiation and describes photon flux measurements which we have made on the 4° beam line at the Stanford Synchrotron Radiation Laboratory (SSRL). In Chapter II experiments are presented and discussed with respect to atomic cross-section effects in soft-x-ray photoemission. By virtue of this atomic cross-section contribution, the study of adsorbate molecular orbitals becomes feasible at photon energies above $\hbar\omega \geq 80$ eV. Thusly, we report a closely related experiment, angle-integrated photoemission studies of the molecular orbitals of CO on Pt(111) using 40 - 150 eV synchrotron radiation in Chapter III.

When the sample is a single crystal with a fixed orientation in space, the angle of the polarization of the light with respect to the sample becomes very important. Polarization of the incident light source can be useful for probing the spatial anisotropies of the sample. With a single crystal sample there is also an anisotropic emission of electrons, so that the number of photoemitted electrons at kinetic energy E_{ke} will be given by

$$I \propto \sigma_i \ (\hbar\omega, E_{ke}, \vec{q}, \vec{A}) \quad . \tag{1}$$

$\vec{q}$ is the vector momentum of the photoemitted electron and $\vec{A}$ is the polarization vector, where both directions are measured with respect to the surface normal and the crystal orientation within the surface plane. The symbol σ_i stands for the angular dependent partial photoionization cross-section for the formation of a given ionic state

whose energy relative to E_0, the ground state of the neutral is

$$E(\text{ion}) = \hbar\omega - E_{ke} - E_0 \quad . \tag{2}$$

A specific state of the ion is denoted by its binding energy

$$E_B^i = \hbar\omega - E_{ke} \quad . \tag{3}$$

In the photoemission technique the detection of a peak in intensity at a given kinetic energy measurement implies the observation of a specific ionic state.[2] These binding energies can be related to a large degree to the ground electronic state, via Koopmans' Theorem.[3] Thus, photoemission permits the study of "one-electron density of states" (N(E)), as well as atomic and molecular orbitals.

When a gas-phase atom or molecule chemisorbs to a substrate surface there is a fundamental difference that takes place in the resulting photoemission intensity. In the gas phase the molecule is randomly oriented and the differential photoemission cross-section[4] may be described as

$$d\sigma/d\Omega = \sigma/4\pi \; [1 + \beta P_2(\cos\theta)] \tag{4}$$

where σ is the total cross-section, β is the asymmetry parameter characterizing the angular distribution from the final ionic state and $P_2(\cos\theta) = 3(\cos^2\theta - 1)/2$. θ is the angle between the photoelectron momentum ($\vec{q}$) and the polarization vector of the light. However, for a chemisorbed molecule, the orientation is not random and a form for the photoemission intensity as in equation (1) must

be maintained. This is a much more complicated expression to describe and evaluate in detail, but more information is available as a result.

The remainder of the thesis will deal primarily with oriented adsorbate photoemission intensity. The uniqueness of synchrotron radiation for studies such as these is that it allows one to measure the σ_i's as continuous functions of $\hbar\omega$, $\vec{q}$, and $\vec{A}$. Chapter IV presents and discusses experiments which are conducted at photon energies where the orientation of a molecular adsorbate with respect to a single crystal surface can be determined. In Chapter V synchrotron radiation studies for CO on Pt(111) at higher photon energies are presented and discussed within the framework of determining surface site geometry.

REFERENCES

1. For a recent review see D. E. Eastman, in Proc. IV International Conference on Vacuum Ultraviolet Radiation Physics, Hamburg, July 1974, ed. E. Koch, R. Haensel, and C. Kunz (Pergamon, Vieweg 1974).
2. This excludes peaks in the kinetic energy distribution which originate from Auger transitions.
3. T. Koopmans, Physica 1, 104 (1933). In short Koopmans' Theorem states that if one neglects the readjustment of the orbitals resulting from ionization, the absolute value of the Hartree-Fock eigenvalue (ε_{ii}) equals the energy needed to remove an electron from the ith atomic or molecular orbital.
4. D. J. Kennedy and S. T. Manson, Phys. Rev. A5, 227 (1972).

I. PHOTON SOURCES

A. Laboratory and Synchrotron Photon Sources

Historically, there has been an artificial separation of the vacuum-ultraviolet (VUV) and x-ray regime of photoelectron spectroscopy (PES). The best laboratory sources of photons for PES are in the energy range 10 eV ~ 10^4 eV and have been either resonance lines in gas discharges or characteristic x-ray lines. As a result, only widely separated, non-tunable, discrete energies are available. Common gas discharge sources yield photons of from ~10.2 eV for the H(Lyman α) line to ~40.8 eV for HeII radiation. On the high energy side of the spectrum AlKα (1486.6 eV) and MgKα (1253.6 eV) characteristic x-ray lines have been employed. Table I summarizes several sources which are employed in this Laboratory. More recently there has been success in utilizing NaKα (1041.0 eV) and YMζ (132.3 eV) x-rays, especially for the study of molecular orbitals in gases.[1]

The spectral range between roughly 20 eV and 1000 eV has remained essentially closed until the advent of conveniently usable synchrotron light sources. The photon regime within this energy range is of interest because all valence orbitals in atoms, molecules, and solids become accessible to photons of energy $\hbar\omega \geq 50$ eV. The K-edges of the chemically important second-row elements C, N, O, and F are reached at $\hbar\omega \leq 700$ eV, and the neon K-edge is accessible at $\hbar\omega \geq 870$ eV. A light source, continuously tunable over this range, allows both absorption

and photoemission measurements to be conducted from the resonant threshold of these levels to higher energies.

The effective sampling depth for the photoemission technique also varies with the kinetic energy of the photoemitted electron. The photon penetration depth is sufficiently deep that it can be neglected in determining surface sensitivity, unless extremely grazing incidence angles are employed. Electromagnetic radiation for photon energies at and above the visible frequencies penetrate a solid for distances of approximately 10^4 Å.[2] A "Universal Curve" of sampling depth versus electron energy is shown in Fig. 1. Electron mean free paths between loss events are seen to be minimum in metals for electron kinetic energies between 50 eV and 200 eV, dropping to 2 ~ 5 Å in this range. Thus for photons of sufficiently high energy to eject a core level electron or valence band electron to kinetic energies within this energy window photoemission spectra are highly sensitive to the atomic surface. This curve represents a wide range of data on effective sampling depths in heavy metals, compiled from many literature sources; C. R. Brundle[3] has compiled a recent list of sources.

The basic properties of synchrotron radiation in comparison with other sources of electromagnetic radiation have been explained in detail[4,5]; however, they may be summarized as follows, especially as they pertain to the SSRL (Stanford Synchrotron Radiation Laboratory) facility located on the storage ring SPEAR:

a. Broad Spectral Bandwidth radiated as a smooth, featureless continuum without the structure associated with laboratory sources.

b. High degree of collimation (with a small source size) which is associated with the relativistic energies of the electrons traveling in circular motion.

c. High Intensity over much of the spectral distribution.

d. High degree of polarization resulting from the relativistic energies of the electron beam.

e. Pulsed time structure.

Figure 2 shows the spectral distribution[4] of synchrotron radiation from the SPEAR electron-positron storage ring and indicates the region of the spectral distribution which is available for photoemission studies. The limitations of this energy region are determined by the monochromator's mechanical motions at low energies and by the carbon K-absorption edge at the high energy side, resulting from hydrocarbon contamination of the reflecting surfaces.

B. Photon Flux Measurements of Monochromatized Light from 32 eV - 650 eV.

Our experiments involving synchrotron radiation were performed on the 4° beam-line at SSRL. Two mrad. of the synchrotron radiation are deflected horizontally by a platinum coated copper mirror[6] onto the entrance slit of the monochromator located 15 meters from the source point. Two mirrors have been used during the past several years: the first one had an RMS roughness of 186 ± 14 Å and a more recent version is in use now with a roughness of 38.9 ± 1.6 Å.[7] The monochromator accepts light at grazing incidence and is capable of operating at $\leq 10^{-10}$ Torr. The exit beam leaves the monochromator at a constant

angle from a fixed exit slit, to be focused by a gold-plated cylindrical quartz section onto the sample with a focal spot size of ~ 1x3 mm. Further details are given in the paper by Brown et al.[8] The monochromator has been designed to operate at a constant resolution of 0.1 Å and is capable of providing monochromatic radiation from 32 eV to 650 eV. The monochromator's design resolution is related to the photon energy by

$$\Delta E(eV) = 8\times10^{-6}(\hbar\omega)^2 \qquad (1)$$

where both ΔE and $\hbar\omega$ are in units of eV. Table II summarizes the resolution for various energy settings. The monochromator supplies reasonable ($\lesssim$ 0.5 eV) resolution and intensity over the range 32 eV $\lesssim$ $\hbar\omega$ $\lesssim$ 250 eV.

We have made spectral distribution measurements on the SSRL 4° beam line for photon energies from 32 eV up to about 650 eV. Although the theoretical resolution ΔE of this instrument is a band pass of 0.1 Å, photoemission studies of several core levels have shown that the resolution was roughly a factor of two larger than the design value[9] during the periods of our use. An NBS - Al_2O_3 photodiode[10], which is schematically shown in Fig. 3a, was used for the transmission measurements. The resulting curve is shown in Fig. 3b. In order to obtain the true transmission function, the curve would have to be corrected by the quantum efficiency of Al_2O_3 which is shown to vary by ~ 50% over the range 40 eV to 155 eV[11]. Figure 3b also exhibits very clearly the intensity modulation produced by the carbon contamination of the optical elements above ~ 285 eV.

The photodiode is seen to have two operating elements: an anode which is a stainless steel cylinder and a cathode consisting of a quartz substrate supporting an aluminum evaporated film which has been anodized to an oxide thickness of approximately 150 Å. We have operated the anode at +60.0 V as recommended by NBS. Since a significant number of photoelectrons which leave the cathode do not arrive at the anode, the photocurrent was measured from the cathode using a Model 417 Keithly high speed picoammeter. The proportional output voltage of the picoammeter was input into a volgate to frequency converter, which produced a signal stored as counts in a multichannel analyzer. The linearity of these cathodes has been proven to photon fluxes of $\sim 10^{11}/sec^{10}$.

Absolute photon flux measurements can be performed from 32 eV to 66 eV, the limit for the NBS calibration. Table IV gives a compilation of the calibrated photon flux for the 4° beam line, as the number of photons mA^{-1} sec^{-1}. The quantum efficiency values above $\hbar\omega \approx 66$ eV have been determined by normalizing Gudat, et al.[11] photo-yield measurements to the NBS reference for two values, $\hbar\omega = 50$ eV and 60 eV. Interpolations were then made from Ref. 11 Fig. 3 for the quantum yield up to $\hbar\omega = 155$ eV (cf. Fig. 4).

It is slightly unfair to compare the spectral throughput at a constant 0.2 Å bandpass for the 4° beam line monochromator against the spectra distributions typically quoted for storage rings. The SPEAR intensity distribution at ~3 GeV beam energies is 2×10^{12} and 5×10^{12} photons sec^{-1} $mrad^{-1}$ mA^{-1} (10% bandwidth)$^{-1}$ at $\hbar\omega = 60$ eV and 290 eV, respectively. Our photon flux measurements integrated to yield a 10% bandwidth are 1.9×10^{9} and 1.6×10^{8}, respectively. Hence, the

monochromator efficiency is approximately 0.1% efficient at $\hbar\omega$ = 60 eV while the efficiency at $\hbar\omega$ = 290 eV is about 0.003%.

The development of a high resolution, high throughput monochromator which covers a wider range 10 - 1500 eV has recently been proposed by H. W. Schnopper and L. Van Speybroeck[12]. Instead of employing a grazing incidence reflection grating, they have proposed the use of a transmission grating. The design has been tested at SSRL and may represent a future monochromator for new beam lines. Other possibilities may include large d-spacing-crystal monochromators to attain high photon energies[13].

C. He Discharge Lamps and Soft X-ray Tubes

Laboratory sources such as differentially pumped discharge lamps utilizing rare gases at low pressures and low energy x-ray tubes have provided useful sources of radiation for the study of atoms, molecules, and solids[14]. Although these sources are restricted, as mentioned earlier, to discrete lines, their advantage in comparison with synchrotron sources is that they are inexpensive, easily operated, and do not impose a severe time table for experiments. Some limitations exist because the emitted photon spectra are composed of several lines which are simultaneously incident upon the sample. Hence, the interpretation of the photoemission energy distributions in certain cases can be complicated by the overlap of spectra from more than one photon line.

In the experiments with x-rays we have employed a modified Hewlett-Packard 5950A electron spectrometer with a total instrumental

resolution of 0.55 eV. The AlKα source is monochromatized by means of a dispersion compensation scheme[15]. Our use of the He discharge lamp has not necessitated use of closely spaced lines. The He I line and the He II line generally are isolated sufficiently in energy for most experiments. To observe core levels with He II radiation we have occasionally used carbon films of ~ 18 $\mu g/cm^2$ to filter out most of the He I radiation. Polymer films have also been successfully employed[16].

REFERENCES

1. M. S. Banna, Ph.D. Thesis, University of California, Lawrence Berkeley Laboratory Report, LBL-3473 (1975), unpublished.
2. C. B. Duke in Advances in Chemical Physics, Vol. XXVII, edited by I. Prigogine and S. A. Rice (Interscience), p. 9 and references therein.
3. C. R. Brundle, Surface Science 48, 99 (1975).
4. S. Doniach, I. Lindau, W. E. Spicer, and H. Winick, J. Vac. Sci. Technol. 12, 1123 (1975).
5. For a review of synchrotron facilities: M. L. Perlman, E. M. Rowe, and R. E. Watson, Physics Today, p. 32, July 1974.
6. J. L. Stanford, V. Rehn, D. S. Kyser, and V. O. Jones in Proceedings of the Fourth International Conference on Vacuum Ultraviolet Radiation Physics, Hamburg, July 1974, edited by E. Koch, R. Haensel, and C. Kunz (Pergamon, Vieweg, 1974), p. 783.
7. R. Z. Bachrach, S. A. Flodström, R. S. Bauer, V. Rehn, and V. O. Jones, Third Annual SSRP Users Group Meeting, SSRP Report No. 76/11, October 28-30, 1976.
8. F. C. Brown, R. Z. Bachrach, S.B.M. Hagström, N. Lien, and C. H. Pruett, Ref. 6, p. 785.
9. At high photon energies ($\hbar\omega \approx 70$ eV) where core levels were measured imperfections in the gratings and on the reflecting mirror surfaces appear to increase the resolution over the 0.1 Å bandpass value.

10. E. B. Saloman and D. L. Ederer, Applied Optics, 14, 1029 (1975); R. P. Madden, NBS Report of Calibration (unpublished).

11. W. Gudat, C. Kunz, and W. Lenth, Ref. 6, p. 725.

12. H. W. Schnopper, L. P. Van Speybroeck, J. P. Delvaille, A. Epstein, E. Källne, R. Z. Bachrach, J. Dijkstra, and L. Lantwaard, submitted to Applied Optics.

13. Proposal to the National Science Foundation for Beam Line III Advance Planning, Engineering and Construction at SSRP, Feb. 1977.

14. (Gaseous atom and molecules) K. Siegbahn, C. Nordling, G. Johansson, J. Hedman, P. F. Heden, K. Hamrin, U. Gelius, T. Bergmark, L. O. Werme, R. Manne, and Y. Baer, ESCA Applied to Free Molecules, (North-Holland Publ. Co., Amsterdam, 1969). (Transient species) S. T. Lee, Ph.D. Thesis "Unconventional Photoelectron Spectroscopic Studies: PES on Some Transient Species and Reactive Molecules", Univ. of Brit. Columbia, 1974, unpublished. (Metal vapors) S. Suzer and D. A. Shirley, J. Chem. Phys. 61, 2481 (1974); S. Suzer, Ph.D. Thesis, University of California, Lawrence Berkeley Laboratory Report, LBL - 4922 (1976), unpublished. (Solids) S. P. Kowalczyk, Ph.D. Thesis, University of California, Lawrence Berkeley Laboratory Report, LBL - 4319 (1976) and references therein, unpublished.

15. K. Siegbahn, D. Hammond, H. Fellner-Feldegg, and E. F. Barnett, Science 176, 245 (1972) and references therein; M. A. Kelly and C. E. Tyler, Hewlett-Packard Journal 24, 2 (1973).

16. P. R. Norton and P. J. Richards, Chem. Phys. Lett. 38, 92 (1976).

TABLE I. Laboratory Photon Sources

Energies of Common Photon Sources	
Source	Energy (eV)
He I	21.22*
He II	40.81*
YMζ	132.3
NaK$\alpha_{1,2}$	1041.0
MgK$\alpha_{1,2}$	1253.6
AlK$\alpha_{1,2}$	1486.6

* Strongest components of the gas-discharge for photoemission.

Kα lines result from 1s - 2p transitions.

Mζ lines result from $3d_{5/2} - 4p_{3/2}$ transitions.

TABLE II. SSRL 4° Beam Line - Monochromator Resolution.

Photon Energy $\hbar\omega$ (eV)	Monochromator Resolution $E(eV) = 8 \times 10^{-6}(\hbar\omega)^2$ *
32	0.008
40	0.013
60	0.03
80	0.05
100	0.08
120	0.12
140	0.16
160	0.21
180	0.26
200	0.32
250	0.50
300	0.72
350	0.98

* This equation is representative of a constant resolution of 0.1Å.

TABLE III. Quantum Efficiency for the NBS Windowless Far UV Photodiode.

Wavelength (Å)	Energy (eV)	Quantum Efficiency*
1216	10.2	0.00799
1026	12.1	0.0448
920	13.5	0.0770
865	14.3	0.0887
818	15.2	0.106
735	16.9	0.147
669	18.5	0.156
584	21.2	0.137
563	22.0	0.132
542	22.9	0.123
521	23.8	0.135
500	24.8	0.119
479	25.9	0.124
458	27.1	0.119
438	28.3	0.114
417	29.7	0.117
396	31.3	0.113
375	33.1	0.111
354	35.0	0.107
333	37.2	0.105
313	39.6	0.097
292	42.5	0.087
271	45.8	0.082
250	49.6	0.079
229	54.1	0.073
208	59.6	0.071
188	66.0	0.067

*Calibration uncertainties are about 10%.

TABLE IV: Photon Flux Measurements for SSRL 4° Beam Line

E(eV)	mA in ring	A on pAmeter(10^{-12})	Q	photons $sec^{-1}mA^{-1}(10^7)$
+32	34.466	6.25	.112	1.01
35	34.292	7.30	.107	1.24
37	34.170	7.80	.105	1.36
40	34.087	9.25	.096	1.76
43	33.809	10.3	.086	2.21
46	33.700	10.9	.082	2.46
50	33.621	13.0	.079	3.06
54	33.559	12.9	.073	3.29
60	33.464	13.9	.071	3.65
66	33.338	16.1	.067	4.50
*70	32.464	17.3	.062	5.36
80	32.355	24.7	.070	6.81
90	32.231	24.8	.060	8.00
100	32.079	40.0	.083	9.37
110	32.002	41.0	.070	11.4
120	31.927	45.5	.067	13.3
130	31.851	51.5	.067	15.1
140	31.760	54.5	.063	17.0
150	31.670	55.0	.060	18.1
160	31.609	51.5	.05	20.3
170	31.504	43.5	.05	17.2
180	31.444	36.5	.05	14.5
190	31.354	32.0	.05	12.7
200	31.041	29.5	.05	11.9
220	30.982	26.0	.05	10.5
240	30.894	23.2	.05	9.37
250	30.835	21.6	.05	8.74
260	30.792	19.4	.05	7.86
270	30.704	17.0	.05	6.91
280	30.646	10.3	.05	4.19
290	30.444	3.60	.05	1.48
300	30.400	4.25	.05	1.75

+ For energies between 32 eV and 66 eV the Quantum efficiency (Q) has been calibrated by NBS. (Ref. 10).

* For energies between 70 eV and 155 eV the Quantum efficiencies were taken from Ref. 11 and normalized to NBS values as described in this chapter.
The Quantum efficiencies were assumed 0.05 for all photon energies higher than 155 eV.

FIGURE CAPTIONS

Fig. 1 The "Universal Curve" for electron attenuation length. A band is drawn to represent that there is a spread due to the nature of various solids. The energies of several laboratory photon sources are shown for reference.

Fig. 2 Spectral distribution of synchrotron radiation emitted from the storage ring, SPEAR. The bracketed region represents the photon energies accessible from the 4° beam line. Photon detection techniques are more sensitive to low fluxes and can be extended beyond that available to photoemission studies.

Fig. 3 a) Schematic of the NBS - Al_2O_3 photodiode. b) Relative photocurrent from an NBS - Al_2O_3 photodiode is plotted against the photon energy range accessible to the 4° beam line monochromator. Absolute yields must be corrected for detector quantum efficiency.

Fig. 4 Photoelectric yield data (Ref. 11) for photon energies above 66 eV normalized to the quantum efficiency of calibrated NBS - Al_2O_3 photodiode (Ref. 10).

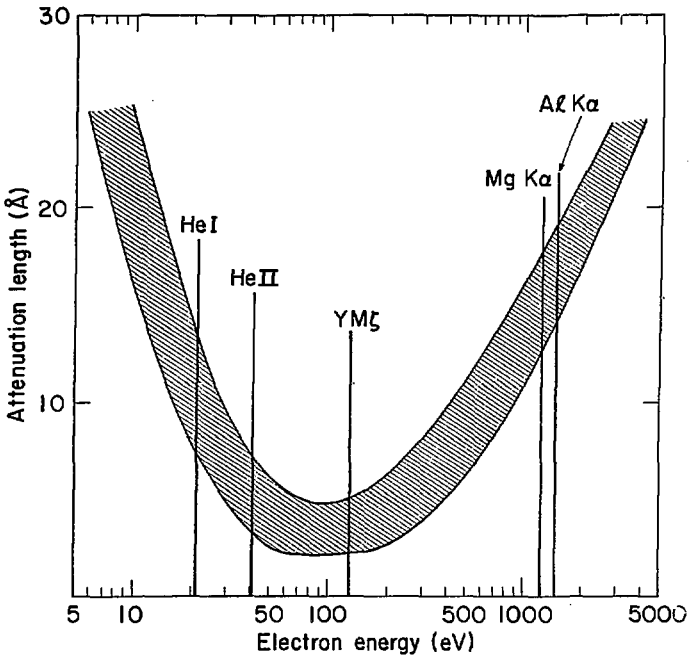
30
20
10
Attenuation length (Å)
HeI
HeII
YMζ
Mg Kα
Aℓ Kα
5
10
50
100
500
1000
5000
Electron energy (eV)
XBL 755-3056

Fig. 1

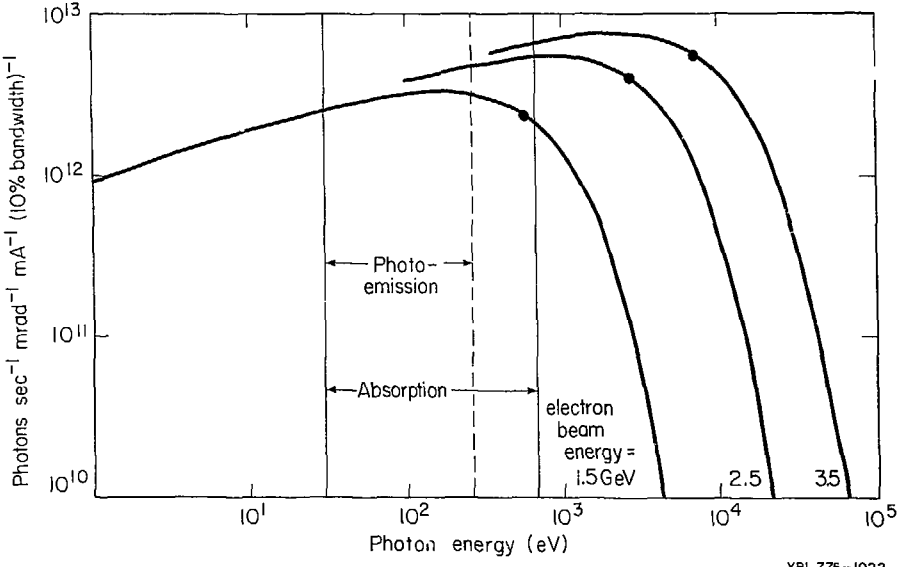
10^{13}
10^{12}
10^{11}
10^{10}
Photons sec^{-1} $mrad^{-1}$ mA^{-1} (10% bandwidth)$^{-1}$
Photo-
emission
Absorption
electron
beam
energy =
1.5GeV
2.5
3.5
10^{1}
10^{2}
10^{3}
10^{4}
10^{5}
Photon energy (eV)
XBL 775-1022

Fig. 2

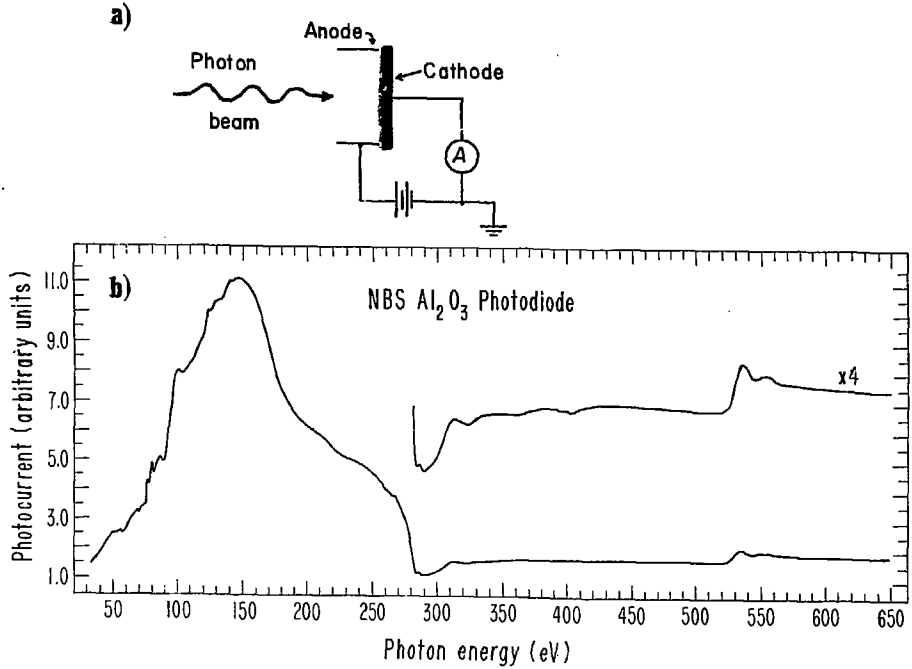

Fig. 3

XBL 775-8634

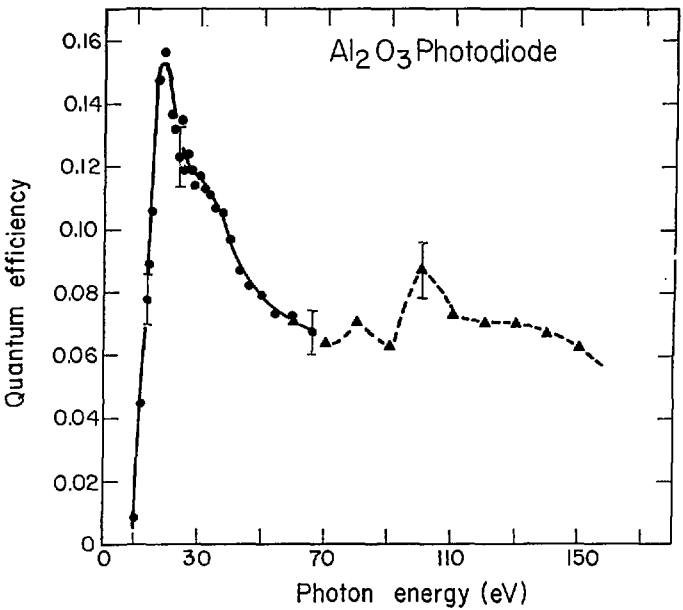

Fig. 4

XBL 775-1019

ANGLE-INTEGRATED PHOTOEMISSION MEASUREMENTS

II. ATOMIC CROSS SECTION EFFECTS IN SOFT X-RAY PHOTOEMISSION FROM Ag AND Au VALENCE BANDS*

ABSTRACT

The relative photoemission intensity from Cu(3d), Ag(4d), and Au(5d) valence bands (VB) was studied as a function of photon energy using 32- 250 eV synchrotron radiation. Studies of the present kind are of interest because it is known from atomic calculations that so-called "Cooper minima" exist in the atomic cross-section for initial state wave functions which exhibit a radial node. In such cases the cross-section may vary strongly over a small energy range. An objective of this study is to investigate whether such effects can be observed in photoemission from 4d (one radial node) and 5d (two radial nodes) initial states. Major emphasis will be given to the Ag (4d) cross-section measurements, which exhibit a sharp decrease in intensity of more than an order of magnitude from 100 eV < $h\omega$ < 140 eV. At $h\omega$ = 140 eV the 4d cross-section exhibits a minimum which is attributed to the radial node of the 4d wavefunction. Modulation of peak intensities in high resolution VB spectra in the energy range 60 eV $\leq h\omega \leq$ 150 eV is related to the atomic cross-section effect. The energy dependence of the Au 5d intensity has been measured and is found to decrease by a factor of ~50 over the investigated photon range 40 - 190 eV. Cu, having no radial nodes in the VB, exhibits no minimum in cross-section.

---

*Based upon work in collaboration with J. Stöhr, P. S. Wehner, R. S. Williams, F. R. McFeely, and D. A. Shirley and published in part in Phys. Rev. B15, 2411 (1976).

A. Introduction

The potential of synchrotron radiation for photoemission studies of solids has long been recognized. So far, however, most studies have been restricted to the photon energy range $\hbar\omega < 100$ eV.[1] The Stanford Synchrotron Radiation Laboratory (SSRL),[2] on the storage ring SPEAR at the Stanford Linear Accelerator (SLAC), is uniquely capable of producing variable-energy photon beams of energies up to 250 eV in sufficient intensity and resolution for photoemission spectroscopy. Here we report a study of the total valence band (VB) intensities of Cu, Ag, and Au in the photon energy range 32 - 250 eV which represents an extension of earlier studies on polycrystalline Cu. The main concern of that study was the extent to which photoemission energy distributions (PED's) from valence bands depend upon the initial density of states, the final density of states, and the photoemission matrix elements.

In general for ultraviolet photoemission spectroscopy (UPS) variations in the PED's at a given photon energy have been discussed in terms of final state effects which are responsible for the observed line positions and the transition matrix element modulations which determine the line intensities.[3] The low energies are dominated by transitions occurring only at special $\vec{k}$ points in the Brillouin zone (BZ) due to the lack of available final states. However, at higher energies ($\hbar\omega > 30$ eV) the number of accessible final states increases[4] so that a considerably larger portion of the BZ is sampled. Therefore the positions of the peaks which constitute the PED predominately reflect the initial density-of-states structure and remain essentially

unshifted. In this regime the three step model of photoemission[1] including strict momentum and energy conservation during the excitation process has proven to describe the experimental situation quite well. For photon energies producing photoelectron kinetic energies near the minimum of the "Universal Curve", momentum broadening in the final state has been used to explain a weakening in intensity modulations.[3,5] The general consensus for polycrystalline samples before this study was that the photoemission energy distributions converge to the initial density of states for photon energies $\hbar\omega > 80$ eV. Below this energy region we have called the modulations in intensity "band-structure-type" cross-section effects.

An example of what has just been discussed is shown in Fig. 1 with a display of the results for polycrystalline Cu.[5] Common features of all spectra are the three peaks at ~2.5 eV, ~3.6 eV, and ~4.7 eV binding energy (BE) relative to the Fermi level. The most distinct changes in the shape of the VB spectra occur between 50 and 70 eV. While the peak positions remain essentially unshifted the intensity of the peak at 3.6 eV BE increases with photon energy. Above 70 eV this trend continues in a less spectacular way. By 80 eV the spectrum seems to approach the PED observed with AlKα radiation[6] which is representative of the initial density of states.

While such "band-structure-type" cross-section effects are also anticipated for Ag and Au, an additional "atomic-type" cross-section effect may be expected. The latter arises from the radial node(s) in the Ag 4d and Au 5d wavefunctions. It is known from atomic calculations[7] that so-called "Cooper minima"[8,9] exist in the cross section for initial-

state wavefunctions which exhibit radial nodes. In such cases the cross-section may vary strongly over a small energy range. One objective of this chapter is to investigate whether such effects can be observed in photoemission from Ag and Au valence bands. Two different kinds of measurements are reported. First we investigate the variation of the effective total photoelectron intensity from the Ag 4d VB in the photon energy range 32 eV $\leq \hbar\omega \leq$ 250 eV, from the Au 5d VB (40 eV $\leq \hbar\omega \leq$ 250 eV), and from the Cu 3d VB (40 eV $\leq \hbar\omega \leq$ 250 eV). Secondly, we report high resolution VB spectra in the energy range 60 eV $\leq \hbar\omega \leq$ 150 eV for Ag. The two sets of results for Ag are then combined and interpreted to deduce how the detailed shape of the Ag VB is affected by atomic-type cross-section effects.

B. Experiments

Experiments were performed using synchrotron radiation from the storage ring SPEAR at SLAC.[2] The incident monochromatic[10] light was focused onto the samples which were positioned in the focal point of a double-pass cylindrical mirror analyzer (CMA). The polycrystalline Ag and Cu samples were prepared by in situ evaporation from a tungsten filament onto a stainless-steel substrate. The Au sample was a polycrystalline foil which was cleaned by argon bombardment and subsequently annealed by heating with an electron gun to remove surface damage. Base pressure in the sample chamber was $<1\times10^{-9}$ Torr, with a maximum pressure of 2×10^{-8} during evaporation. The energy distributions of the photoemitted electrons were analyzed by operating the CMA in the retarding mode.[11] The kinetic energy of the photoelectrons is

modified by the retarding (accelerating) voltage such that only those electrons are detected which have the correct pass energy (E_p) of the analyzer. For a given E_p the resolution ΔE of the CMA is fixed. The variation of the total Cu 3d, Ag 4d, and Au 5d intensities with photon energy was studied with an analyzer resolution of $\Delta E = 1.6$ eV, at $E_p = 100$ eV. High resolution VB spectra of Ag were recorded with a resolution of $\Delta E = 0.35$ eV, at $E_p = 50$ eV.[12]

C. Results

1. Ag

Results of our high resolution studies of the Ag valence bands in the photon energy range 60 eV $\leq h\omega \leq$ 150 eV are shown in Fig. 2. Characteristic features are the flat s-band extending beyond 3 eV BE below the Fermi level and the two prominent d-peaks centered at ~4.8 eV and ~6.3 eV BE, respectively. At the lowest and highest photon energies the d-band structure roughly resembles the x-ray photoemission spectrum (XPS) in Fig. 3 which was taken with AlKα (1486.6 eV) radiation on a Hewlett-Packard 5950A spectrometer. The s-band intensity of all spectra in Fig. 2 is reduced relative to the XPS result, by a factor of approximately 3.[13a] The most prominent changes in the shape of the 4d valence band occur in the energy range 110 eV - 130 eV. Here, the relative heights of the two leading d-peaks are inverted relative to the lower and higher photon energy range.[13b]

The variation of the Ag 4d intensity with photon energy, shown in Fig. 4, was derived in the following way. The experimental spectra

were corrected for their inelastic background. The Ag 4d peak region was defined as 3 eV $\leq$ BE $\leq$ 8 eV. The intensity of the d-band in this energy range was estimated by extrapolating the s-band intensity for BE $\geq$ 3 eV and substracting it from the total intensity. The area obtained this way for the 4d band was normalized with respect to the average photon flux incident on the sample. The photon flux depends on both the electron-beam current of SPEAR at the time of measurement and the transmission of the mirror plus monochromator assembly at a given photon energy. The beam current and its decay during data collection (typical time ~ 30 minutes per spectrum) was supplied on line by SPEAR. The transmission of the mirror plus monochromator as a function of photon energy had previously been measured with a sodium salicylate scintillation counter.[14] Finally, the data were corrected for the collecting efficiency of the CMA.[11,15,16] Due to the action of the accelerating/retarding field the collecting efficiency is a function of both the pass energy (E_p) and the kinetic energy (E_k) of the electrons emitted from the sample. The transmitted current in general is theoretically given by $I \sim E_p/E_k$.[11,15] Thus the observed 4d intensity at a given photon energy $\hbar\omega$ was corrected by a factor E_k/E_p where in our case E_p = 100 eV and $E_k = \hbar\omega$ - 10 eV (4d BE + work function = 10 eV). As seen from Fig. 4 the experimental errors of our data points are rather small (~ ± 10%). The largest uncertainty is the correction for the CMA collecting efficiency. The effect of this correction is seen from Fig. 4 where the uncorrected (constant collecting efficiency) 4d intensity is shown for comparison as a dashed line.

2. Au

The energy dependence of the Au 5d VB intensity in the range 40 eV $\leq \hbar\omega \leq$ 190 eV is shown in Fig. 5 as a solid line. For comparison we have also included the Ag 4d VB photoemission intensity variation in the figure. While the d-band intensity is given in arbitrary units, we have normalized the Ag 4d and Au 5d intensities to each other experimentally by comparing the areas under the PED's from Ag and Au at $\hbar\omega$ = 40 eV for a known photon flux. The data points for Au shown in Fig. 5 were obtained by correcting the Au spectra for their inelastic background, measuring the area under the PED's in the BE range 2 eV - 8 eV (excluding s-band intensity), and correcting this area with respect to the incident photon flux and the collecting efficiency of the CMA.

3. Cu

The variation of Cu 3d intensity with photon energy from Fig. 6 is seen to be very different from that observed for either Ag or Au. The curve increases from $\hbar\omega$ = 40 eV to $\sim \hbar\omega$ = 120 eV, then gradually decreases to our highest energy, $\hbar\omega$ = 250 eV. The total Cu VB intensity measurement as a function of energy was performed during a different SSRL running period and utilized the NBS photodiode to measure the transmission of the mirror plus monochromator. The s-band was subtracted from the spectra for the binding energy region of 1.5 - 6 eV.

D. Discussion

Let us first discuss the variation of the Ag 4d intensity with photon energy. The measured intensity of the Ag valence band at a given photon energy [I(ω)] is in general a very complex quantity.

Among other factors that modulate $I(\omega)$ is the effect of electron energy loss during transport to the surface. This effe is most important in just the energy range we have studied. However, it is difficult to assess and is probably a much weaker effect than the atomic cross-section modulation discussed below (the escape depth probably varies by a factor of two or less, while the atomic cross-section varies over an order of magnitude). We shall therefore consider the variation in mean escape depth to be absorbed into an "effective" cross-section variation. For the case of an angle integrated measurement on a polycrystalline sample the observed intensity in this approximation is given by[17]

$$I(\omega) = \frac{C}{f(\omega)} \int dE\ N(\omega,E)$$

$$= \frac{C}{f(\omega)} \int dE \int d^3k \sum_{f,j} |t_{fj}(\vec{k})|^2\ \delta(E_f(\vec{k}) - E_j(\vec{k}) - \hbar\omega)\ \delta(E - E_j(\vec{k})) \qquad (1)$$

Here $N(\omega,E)$ is the photoemission energy distribution (PED) that is usually measured in photoemission experiments (cf. Fig. 2). $t_{fj}(\vec{k})$ is a momentum matrix element for a transition between an initial state j of energy $E_j(\vec{k})$ and a final state f of energy $E_f(\vec{k})$. The $\vec{k}$-integration extends over the first Brillouin zone (BZ). From equation (1) it is seen that in general it is impossible to relate the measured quantity $I(\omega)$ to a single physical parameter. However, such a correspondence can be approximately established if final state effects are weak, i.e. if transitions are allowed throughout the whole BZ and effects arising from the angular part[5] of the matrix element t_{fj} are unimportant.

In this case equation (1) simplifies to[18]

$$I(\omega) = \frac{C}{f(\omega)} \int dE \, \overline{|t_{fj}|^2} \, N_j(E) \, N_f(E + \hbar\omega) \qquad (2)$$

Here $\overline{|t_{fj}|^2}$ is an angle averaged (radial) transition matrix element which depends on the wavevector of the photoelectron $|\vec{q}| = [2m\,(E + \hbar\omega)]^{1/2}/\hbar$.[19] $N_j(E)$ and $N_f(E + \hbar\omega)$ are the initial and final densities of states, respectively. To a good approximation it can usually be assumed that $|t_{fj}|^2$ and N_f are only weakly energy dependent over the range of integration, i.e. over the width of the "d" part of the valence band (~3 eV), provided that the photon energy is sufficiently high. Then the measured intensity is directly proportional to the photo-ionization cross section

$$I(\omega) \sim \sigma(\omega, E_f) \sim \frac{1}{f(\omega)} \overline{|t_{fj}(E_f)|^2} \, N_f(E_f) \quad . \qquad (3)$$

Here $E_f = \bar{E}_j + \hbar\omega$, and $\bar{E}_j$ is taken to be the center of the 4d valence band. $\sigma(\omega)$ has been calculated for various atoms.[7] Unfortunately, at present, no experimental or reliable theoretical results are available for atomic Ag 4d orbitals. A comparison of accurate theoretical atomic cross-sections with the present data might yield useful information on how cross-section effects are modified when the atom is introduced into a solid. In fact, from our previous results for polycrystalline Cu[5] one would expect final state band structure effects to be weak for $\hbar\omega \geq 80$ eV, and therefore equation (3) should hold to a reasonable approximation. In the range $\hbar\omega \leq 80$ eV the curve in Fig. 4 might deviate from a corresponding plot of the atomic Ag 4d cross-section

versus energy because the final state band structure and effects due to the angular part of the transition matrix element come into play.[5] However, since such deviations are closely related to the weak modulation effects seen in extended x-ray absorption fine structure (EXAFS), they might lie within the error bars of our measurement.

The minimum in the curve shown in Fig. 4 arises from the radial matrix element $\overline{|t_{fj}|^2}$ in equation (3)[20] and may be explained as follows. The selection rules for electric dipole transitions($\Delta\ell = \pm 1$) connect the 4d initial state of Ag to p- and f-partial wave final states (channels). In general, a minimum in the cross section can occur provided the initial state wavefunction has at least one node. In this case the radial dipole matrix element associated with the p or the f channel may change sign as a function of photon energy.[21] The photoexcitation cross-section, which is proportional to the sum of the squares of the p and f channel matrix elements,[21] will then exhibit a minimum at the energy for which one of the matrix elements vanishes. Because the absolute value of the $d \rightarrow f$ matrix element dominates the $d \rightarrow p$ one at higher (> 20 eV) kinetic energies[9] the minimum observed for Ag 4d at $\hbar\omega$ = 140 eV may be attributed to a vanishing $d \rightarrow f$ matrix element at this energy. Rather than using a rigorous approach we have calculated the Ag 4d cross section as a function of the kinetic energy of the photoelectron, using plane-wave (PW) and orthogonalized plane-wave (OPW) final states for the continuum electron[22] in order to obtain an intuitive understanding. The results of such calculations for $\overline{|t_{fj}|^2}$ are shown in Fig. 7 for the cases of Cu(3d) and Ag(4d). While neither PW nor OPW can be taken seriously for quantitative estimates of cross-sections, we note that both show deep

minima around $\hbar\omega \approx 140$ eV for Ag. For Cu no such minimum exists. In the simple PW and OPW final state picture the correspondence between a minimum in the cross-section and a radial node in the initial state wavefunction is easily seen. Consider the atomic matrix element for a 3d and a 4d initial state wavefunction and a PW final state:

$$\langle e^{i\vec{q}\cdot\vec{r}} \, |\vec{p}| \, ar^2e^{-\alpha r} + br^3e^{-\beta r} \rangle \qquad (4)$$

Here $\vec{q}$ is the photoelectron wavevector, and the initial state is written in the form of Slater orbitals. For a 3d initial state: $a > 0$, $b \geq 0$; for 4d: $a > 0$, $b < 0$, and a radial node exists. Thus, for a 3d state both parts of the matrix element in equation (4) have the same sign. For a 4d state opposite signs result, and, depending on the magnitude of the two terms the matrix element (4) may change sign as a function of the final state energy ($\sim|\vec{q}|^2$). The square of the matrix element then exhibits a Cooper minimum. While for a PW final state the cross section in a Cooper minimum is zero, it is finite for an OPW due to the orthogonalization terms in the matrix element.[5]

The experimental observation that transitions from d-like initial states to f-like final states are weak near the threshold, showing a broad rise and then a decrease at higher energies can be understood in terms of the radial matrix elements for normalized initial and final continuum wavefunctions. Whereas the simpler PW and OPW treatments do not predict this behavior near threshold, more refined calculations of photoionization from atoms in the soft x-ray range,[7,23] account very well for this behavior. Absorption measurements have also demonstrated these gradual onsets of intensity several tens of eV above threshold.[24]

These effects are attributed to centrifugal repulsion for $\ell = 3$ from the contribution of the $\ell(\ell+1)/r^2$ potential term in the radial Schrödinger equation. Near threshold the εf (ε = continuum electron kinetic energy) radial function is restrained to be far out by the centrifugal repulsion and has little overlap with the 3d, for example. As the kinetic energy increases the εf wavefunction begins to penetrate deeper into the core creating a larger cross section. However, eventually at large energies cancellation in overlap becomes important because of its radial nodes. This causes, for example, the monotonic decrease in intensity for Cu for $\hbar\omega \geq 120$ eV. It appears that the energy position of the intensity maximum beyond threshold can be related to the orbital radial expectation value $\langle r \rangle$, which decreases in the series 3d < 4d < 5d. Maximum overlap beyond threshold for the εf radial function should be at lowest energies for 5d orbitals, increasing to highest energies for 3d orbitals. Experiments verify this (cf. Figs. 5 and 6); the maxima occur as follows: Au 5d, $\hbar\omega < 40$ eV, Ag 4d, $\hbar\omega \approx 70$ eV, and Cu 3d, $\hbar\omega \approx 130$ eV.

In the context of this chapter the curve shown in Fig. 4 is of interest for yet another reason, namely, for its effect on the detailed shape of the Ag VB spectrum (Fig. 2). In particular, we focus our attention on the changes in the energy range $90 \text{ eV} \leq \hbar\omega \leq 150$ eV. At these photon energies "band-structure-type" cross section effects are expected to be weak[5] and may therefore be excluded as being responsible for the observed inversion of peak intensities for $110 \text{ eV} \leq \hbar\omega \leq 130$ eV. On the other hand, the curve shown in Fig. 4 exhibits its largest slope exactly in this latter energy range. As is seen from equation (3) this curve describes in good approximation the dependence of the 4d

cross-section on the final state kinetic energy $E_f = \hbar\omega + E_j$.[25] Earlier, in discussing the energy-integrated quantity $I(\omega)$ we neglected the dependence of t_{fj} and N_f on E_j (equation (3)) by introducing an averaged value $\overline{E}_j$. For the energy-resolved PED's taken at a fixed $\hbar\omega$ the curve in Fig. 4 describes the variation of $\sigma(\omega, E_f)$ over the range of the valence band energies E_j. In the range of steepest slope, i.e. for 100 eV $\leq \hbar\omega \leq$ 130 eV, changes of approximately 20% in $\sigma(\omega, E_f)$ result over an energy interval of $\Delta E_j \sim 2$ eV, which is approximately the separation of the two prominent VB peaks (Fig. 2).[26] Thus in this energy range the effect of the radial matrix element[20] on the detailed shape of the valence band is not negligible. Neglecting "band-structure-type" cross section effects the PED at a given photon energy is described by

$$N(\omega, E) = C \int d^3k \sum_j \sigma(\omega, E_f) \quad \delta(E - E_j(\vec{k})) \qquad . \qquad (5)$$

Figure 8 shows the results of a calculation using equation (5). The solid curve corresponds to the case $\sigma(\omega, E_f) = \text{const}$; i.e. to the density of (initial) states. Details of the calculation are described in ref. 5. Smith's[27] parameters were used with a spin orbit coupling of 0.015 Ry included. The dashed curve was calculated by including the dependence of $\sigma(\omega, E_f)$ on the final state energy. The calculation corresponds to $\hbar\omega$ = 120 eV. The dependence of $\sigma(\omega, E_f)$ was taken from Fig. 4. Inclusion of a final state energy dependent cross section enhances the high BE peak of the Ag 4d valence band by a maximum of 17%. We believe that this effect is responsible for the observed

changes in the shape of the valence-band spectrum in the range 90 - 150 eV. When comparing the slope of the curve in Fig. 4 with the intensity ratio of the two prominent valence band peaks in Fig. 2, the close relationship is apparent. Figure 9 shows the effect more schematically.

We conclude that in the case of polycrystalline silver, even with all the averaging effects that are implied by polycrystallinity and angle-integrated electron detection in our CMA, the transition from a UPS-like to an XPS-like 4d-band spectrum is not complete before 150 eV. If our spectra had been taken with photon energies extending only up to 90 eV, the reversal of intensities would have been overlooked; if to 110 eV, an incorrect density of states might have been inferred. Simil . behavior may be expected in other 4d-group elements. It therefore seems important that valence-band studies on these elements be carried out with photon energies up to at least 150 eV.

The photon energy dependence of photoemission from polycrystalline Au was studied by Freeouf et al.[28] in the range 15 eV $\leq \hbar\omega \leq$ 90 eV. Above $\hbar\omega \approx$ 40 eV the spectral features in the observed PED's did not change significantly. This was discussed by Feibelman and Eastman[3a] in terms of momentum broadening in the final state. Measurements by Lindau et al.[29] up to 200 eV revealed dramatic changes in the shape of the 5d valence band in the range above 100 eV. For example, the intensity ratio of the low (~ 3.5 eV BE) and high (~ 6.5 eV BE) peak decreased from a value of 1.5 at $\hbar\omega$ = 100 eV to 1.0 at $\hbar\omega$ = 120 eV.

Lindau et al. discussed several possible explanations for the observed modulation effects and favored an explanation in terms of an atomic-type cross-section effect. In particular, they associated the two main VB peaks with the spin-orbit-split components $5d_{5/2}$ and $5d_{3/2}$ and argued that the respective cross sections may vary differently with photon energy. We can exclude this explanation on the basis of our experimental results.[30] An atomic type cross-section effect should also be seen in angle-resolved photoemission, i.e. in the range 100 eV $\leq \hbar\omega \leq$ 120 eV for <u>both</u> Au [001] and Au [111]. Inspection of Au single crystal spectra reveal that this is not the case for Au [001].[31] The above argument also excludes an atomic cross-section effect of the Cooper-Fano type as being responsible for the observed modulation effect in Au. This is independently confirmed by the photon energy dependence of the total Au 5d-band intensity (which is in good approximation proportional to the 5d cross section) shown in Fig. 5. In contrast to the case of the 4d intensity in Ag, which exhibits a pronounced Cooper-minimum (cf. Fig. 5), the variation of the Au 5d intensity is not strong enough to significantly influence the shape of the valence band. We note that the PED's for Au [111] show a change in peak amplitudes for 100 eV $\leq \hbar\omega \leq$ 120 eV which goes in the same direction as those observed by Lindau et al.[29] In fact, the low BE peak decreases by a factor of 1.6 from $\hbar\omega$ = 100 eV to $\hbar\omega$ = 120 eV. Similar to the ARP results obtained for Cu, band structure induced cross section effects (i.e. final state plus matrix elements effects) are thus found to be important for angle resolved photoemission from Au

above 100 eV. In the light of the present results preferential orientation of the crystallites in evaporated Au films may cause modulation effects similar to those observed in ref. 29. In fact, such effects were observed for evaporated Au samples by Koyama and Hughey[32] at lower photon energies.

Finally, we briefly comment on band structure type cross section effects which are expected for $\hbar\omega \leq 80$ eV. A close inspection of the spectra in Fig. 2 reveals that the high BE peak is reduced for $\hbar\omega \leq 80$ eV relative to the XPS result (shown in Fig. 3) which should closely represent the initial density of states.[5] This becomes even more apparent when the influence of the inelastic background is taken into account. Similar effects have also been observed for Cu in the 50 - 70 eV range, although the spectral changes are more dramatic for Cu. Also, for Cu the strongest decrease in intensity of the high BE side was observed for $50 \text{ eV} \leq \hbar\omega \leq 60$ eV while for Ag the high BE side is lowest for $\hbar\omega = 80$ eV. The fact that band structure type cross section effects for Ag are weak at the lowest energies studied seems to confirm our interpretation of the effects observed at higher photon energies.

REFERENCES

1. For a review see D. E. Eastman in Vacuum Ultraviolet Radiation Physics, Ed. E. E. Koch, R. Haensel, and C. Kunz (Pergamon, Vieweg 1974) p. 417.

2. H. Winick, in reference 1, p. 776.

3. a) P. J. Fiebelman and D. E. Eastman, Phys. Rev. B10, 4932 (1974); b) W. D. Grobman, D. E. Eastman, and J. L. Freeouf, Phys. Rev. B12, 4405 (1975). c) B. Feuerbacher and R. F. Willis, J. Phys. C, 9, 169 (1976).

4. This is most easily seen for the case of free electron final states where the number of final states increases as the square root of photon energy.

5. J. Stöhr, F. R. McFeely, G. Apai, P. S. Wehner, and D. A. Shirley, Phys. Rev. B14, 4431 (1976).

6. L. Ley, R. A. Pollak, F. R.McFeely, S. P. Kowalczyk, and D. A. Shirley, Phys. Rev. B9, 600 (1974). At XPS energies the final-state energy of the ejected electron is so high that the density of final states is expected to become relatively flat and unstructured and the $\vec{k}$ selection rule is readily fulfilled without introducing additional structure. Evidence for this is available from high energy band-structure calculations of V. Hoffstein and D. S. Boudreaux, Phys. Rev. B2, 3013 (1970).

7. D. J. Kennedy and S. T. Manson, Phys. Rev. A5, 227 (1972).

8. J. W. Cooper, Phys. Rev. Lett. 13, 762 (1964).

9. U. Fano and J. W. Cooper, Rev. Mod. Phys. 40, 441 (1968).

10. F. C. Brown, R. Z. Bachrach, S.B.M. Hagström, N. Lien, and C. H. Pruett in reference 1, p. 785.

11. P. W. Palmberg, J. Electron Spectrosc. 5, 691 (1974).

12. Low (ΔE = 1.6 eV) and high (ΔE = 0.35 eV) resolution spectra were taken with two different CMA's with $\Delta E/E_p$ = 1.6% and 0.7%, respectively.

13. a) The matrix element depends on how well the deBroglie wavelength of the ejected photoelectron "overlaps" with the curvature of the initial-state wavefunction. The electrons in valence s and d bands have different cross sections because of their different radial wavefunctions. The VB's orbitals with a higher number of radial nodes have better overlap with high energy final state electron wavefunctions. b) The rather poor statistics of the spectrum at $\hbar\omega$ = 150 eV are due to a low cross section of the VB in this region (cf. Fig. 4).

14. We are grateful to I. Lindau and P. Pianetta for supplying their results on the monochromator transmission function.

15. J. C. Helmer and N. H. Weichert, Appl. Phys. Lett. 13, 266 (1968).

16. J. L. Gardner and J.A.R. Samson, J. Electron Spectrosc. 2, 267 (1973).

17. See for example reference 1. At the photon energies of this study transport and escape terms may be neglected (cf. reference 5). We have explicitly included a factor $1/f(\omega)$ in eq. (1) which normalizes $N(\omega,E)$ with respect to the incident photon flux.

18. This is easily derived if the selection rules of $\vec{k}$-conservation are ignored and a continuum of final states is assumed. Although it is known that $\vec{k}$-conservation is in general an important selection rule, eq. (2) is still approximately correct at photon energies where final state momentum broadening is important or for the case where the number of final Bloch states is sufficient to lead to an effective angular integration of the transition matrix element (cf. reference 5). Note, however, that the above statements apply only to angle integrated photoemission from polycrystalline samples.

19. See eq. (A17) in reference 5. Here we have neglected the wave-vector dependence of $\overline{|t_{fj}|^2}$, i.e. we have assumed $\sum_m |a_m^j(\vec{k})|^2 = \text{const.}$

20. The final density of states $N_f(E_f) = (E_f)^{1/2}$ cannot be responsible for the strong variations of the curve in Fig. 4.

21. See for example A. M. Msezane and S. T. Manson, Phys. Rev. Lett. 35, 364 (1975) and references 8 and 9. For electrons which move in the same central field, the photoemission cross section is given by

$$\sigma_{n\ell}(\varepsilon) = \frac{4\pi \alpha a_0^2}{2} \frac{N_{n\ell}(\varepsilon - \varepsilon_{n\ell})}{2\ell+1} \left[\ell R^2_{\varepsilon,\ell-1} + (\ell+1) R^2_{\varepsilon,\ell+1}\right] .$$

$\varepsilon_{n\ell}$ = BE (Ry) for an $n\ell$ subshell electron; α = fine structure constant; $N_{n\ell}$ = number of electrons in the subshell; ε = kinetic energy of the ionized electron (Ry). $R_{\varepsilon,\ell\pm1} = \int_0^\infty P_{n\ell}(r)\, r\, P_{\varepsilon,\ell\pm1}(r)\, dr$ where $P_{n\ell}(r)$ and $P_{\varepsilon,\ell\pm1}(r)$ are solutions of the radial Schrödinger equation.

22. We have used eq. (A17) in reference 5 with $\sum_m |a_m^j(\vec{k})|^2 = 1$. The coefficients for the 3d and 4d wavefunctions in form of single zeta Slater orbitals were taken from: E. Clementi and C. Roetti, Atomic Data and Nuclear Data Tables 14, 177 (1974).

23. S. T. Manson and J. W. Cooper, Phys. Rev. 165, 126 (1968).

24. F. C. Brown, Solid State Physics 29, 1 (1974).

25. E_f differs from the kinetic energy of the photoelectron outside the crystal by a work function (~ 4.5 eV for Ag). The energies E_j and E_i are measured relative to the Fermi level $E_F = 0$.

26. Note that the slope of the curve in Fig. 4 in the range 100 eV $\leq$ $\hbar\omega \leq$ 130 eV is almost unaffected by the correction for the analyzer transmission which is somewhat uncertain.

27. N. V. Smith, Phys. Rev. B3, 1862 (1971).

28. J. Freeouf, M. Erbudak, and D. E. Eastman, Solid State Comm. 13, 771 (1973).

29. I. Lindau, P. Pianetta, K. Y. Yu, and W. E. Spicer, Phys. Rev. B13, 492 (1976).

30. We believe that the two Au 5d VB peaks cannot be discussed in terms of the two spin-orbit split components $5d_{3/2}$ and $5d_{5/2}$ since solid-state effects, i.e. band mixing, are dominant.

31. J. Stöhr, G. Apai, P. S. Wehner, F. R. McFeely, R. S. Williams, and D. A. Shirley, Phys. Rev. B14, 5144 (1976).

32. R. Y. Koyama and L. R. Hughey, Phys. Rev. Lett. 29, 1518 (1972).

FIGURE CAPTIONS

Fig. 1 Photoemission spectra of the 3d valence band of Cu for a series of photon energies. Spectra were run at a resolution of $\Delta E = 0.35$ eV.

Fig. 2 Photoemission spectra of Ag (polycrystalline) valence bands in the photon energy range 60 eV $\leq \hbar\omega \leq$ 150 eV. Experimental resolution was 0.35 eV.

Fig. 3 Photoemission spectrum of Ag valence bands at $\hbar\omega = 1486.6$ eV (Aℓ Kα). Experimental resolution was ~ 0.6 eV.

Fig. 4 Relative intensity of the Ag 4d peak as a function of photon energy. The data were collected during three different beam periods (Run 1,2,3). The dashed curve does not include the correction for the collecting efficiency of the cylindrical mirror analyzer as discussed in the text.

Fig. 5 Relative intensity of the 4d valence band of Ag and the 5d valence band of Au as a function of photon energy. The Ag and Au valence band intensities were normalized with respect to each other at $\hbar\omega \approx 40$ eV. (Compare with Fig. 4)

Fig. 6 Relative intensity for the 3d valence band of Cu as a function of photon energy.

Fig. 7 Square of the radial matrix element $\overline{|t_{fj}|^2}$ (reference 22) as a function of the final state kinetic energy E_f (reference 25) for Cu (3d) and Ag (4d). PW and OPW mean plane-wave and orthogonalized plane-wave final states, respectively. The units of $\overline{|t_{fj}|^2}$ are arbitrary but the relative values for Cu and Ag are accurate. The energy scales of Fig. 4 ($\hbar\omega$) and Fig. 7 (E_f) differ by the average initial state energy $\bar{E}_j = -5.5$ eV.

Fig. 8 Calculation of the Ag 4d PED according to eq. (5). The solid line is the density of (initial) states. The dashed curve takes the cross-section dependence on the final state energy $E_f = \hbar\omega + E_j$ into account (Fig. (4)) and corresponds to $\hbar\omega = 120$ eV.

Fig. 9 Illustration of the modulation of peak intensities for the Ag valence band at $\hbar\omega = 110$ eV with respect to the VB density of states. The inversion of peak intensity is attributed to the extremely sharp decrease in overall 4d intensity between 110 eV $\leq \hbar\omega \leq$ 130 eV.

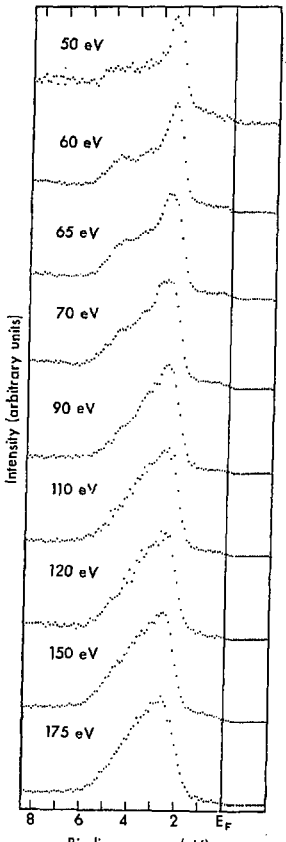

XBL 761 - 2005

Fig. 1

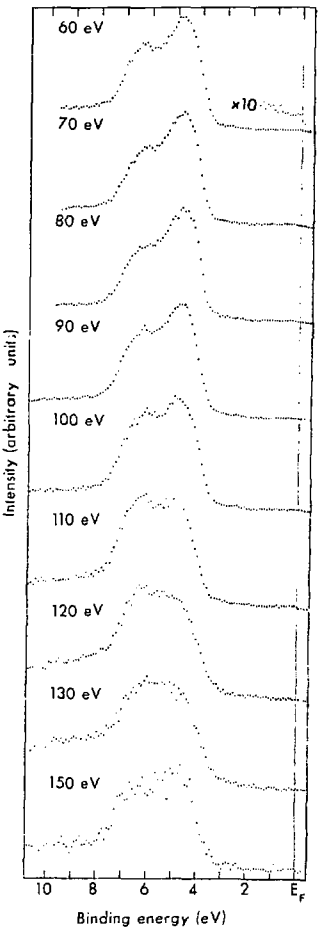
60 eV
70 eV
80 eV
90 eV
100 eV
110 eV
120 eV
130 eV
150 eV
×10
Intensity (arbitrary unit)
10
8
6
4
2
E_F
Binding energy (eV)
XBL761-2006A

Fig. 2

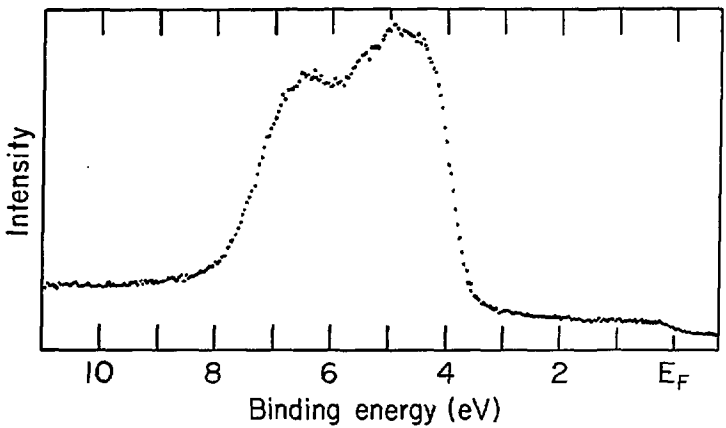

Fig. 3

XBL763-2369

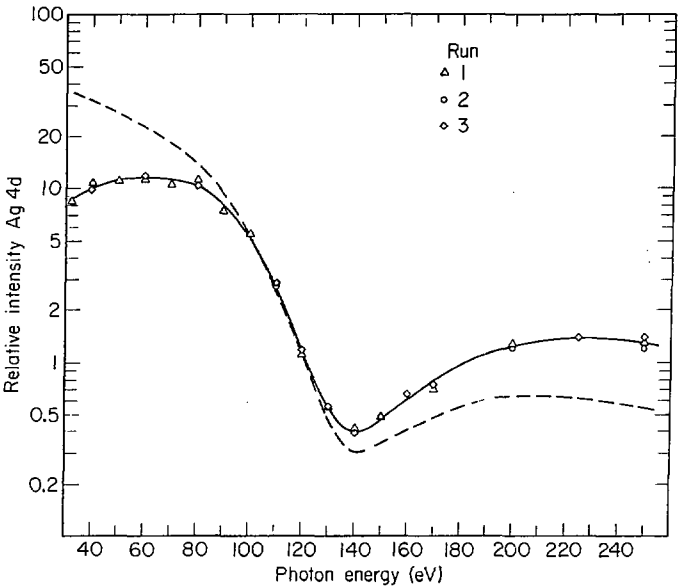

XBL 763-2373

Fig. 4

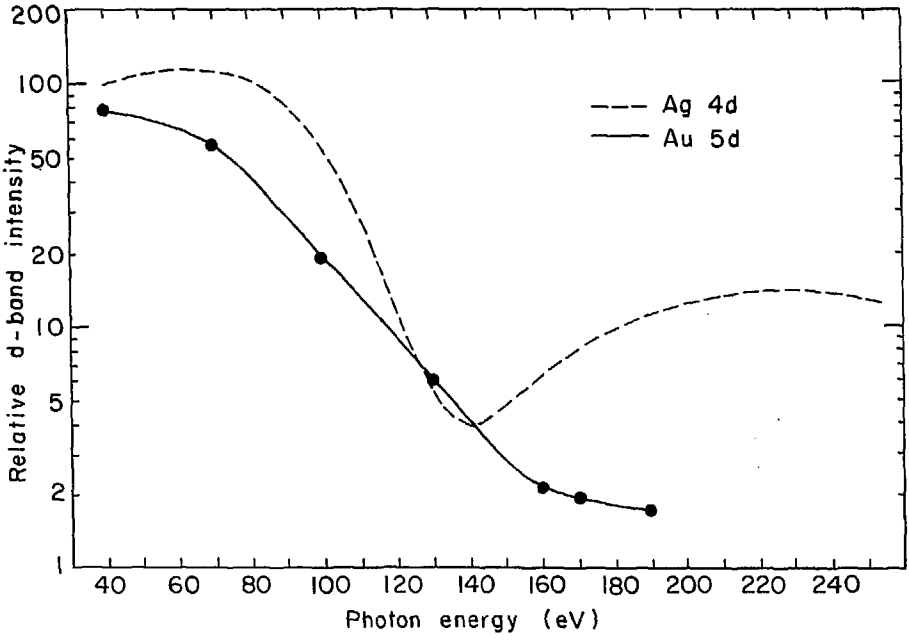

Fig. 5

XBL764-2763

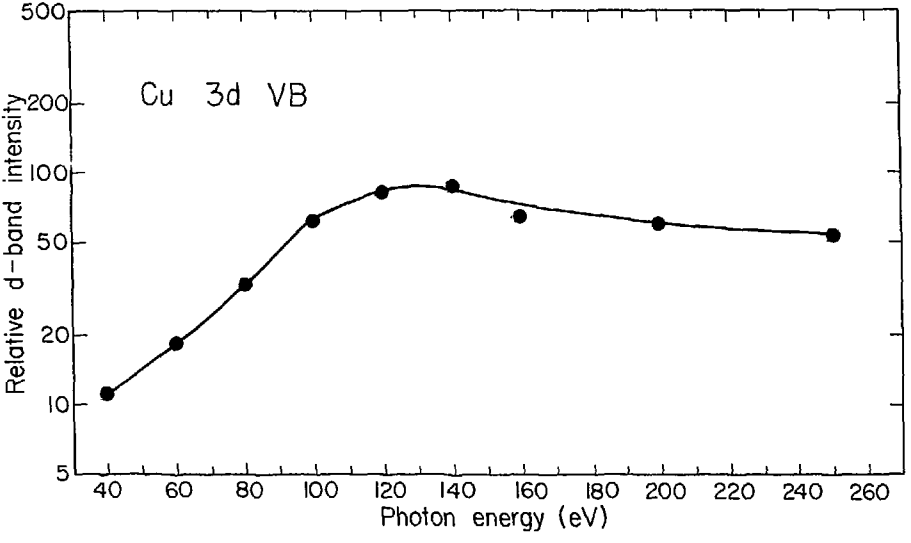

Fig. 6

XBL775-1020

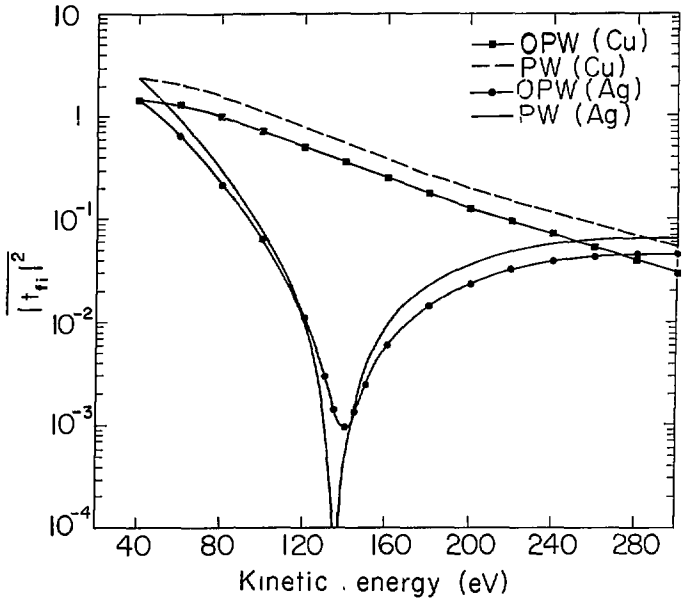
10
1
10^{-1}
10^{-2}
10^{-3}
10^{-4}
$\overline{|t_{fi}|^2}$
40
80
120
160
200
240
280
Kinetic . energy (eV)
OPW (Cu)
PW (Cu)
OPW (Ag)
PW (Ag)
XBL761-2106

Fig. 7

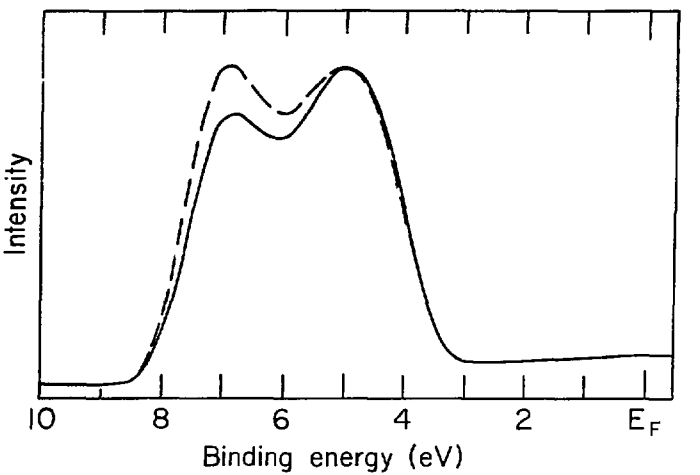

Fig. 8

XBL763-2368

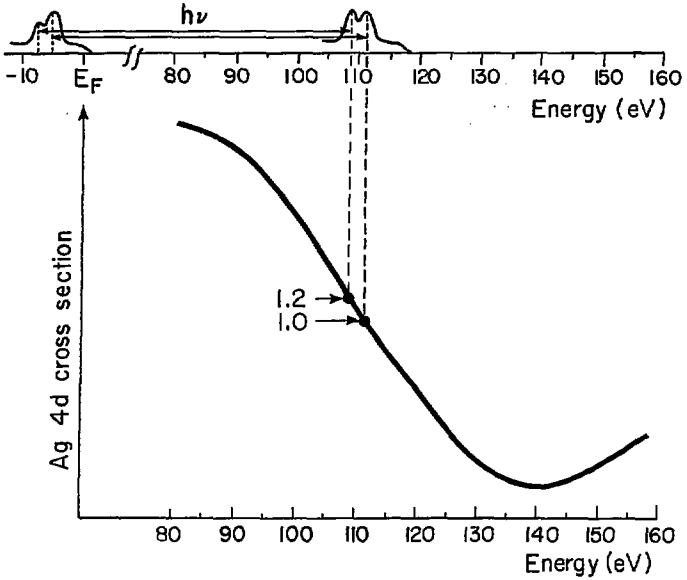

Fig. 9

XBL 775 - 1016

III. PHOTOEMISSION FROM CO ON Pt(111) USING SYNCHROTRON RADIATION IN THE RANGE 40 eV $\leq \hbar\omega \leq$ 150 eV*

ABSTRACT

Photoelectron spectra for CO adsorbed on the (111)-face of Pt have been measured using synchrotron radiation of energy 40 eV $\leq \hbar\omega \leq$ 150 eV. A dramatic increase of the molecular orbital (MO) intensity relative to the intensity of the Pt 5d valence band (VB) is observed for $\hbar\omega > 100$ eV, to a ratio at $\hbar\omega$ = 150 eV that is a factor of three higher than at $\hbar\omega \approx$ 40 eV. The energy variation of the Pt 5d VB photoemission peak intensity has been derived independently in the 40-200 eV range from measurements on clean Pt. The 5d peak intensity is found to decrease steeply (by more than an order of magnitude) between 100 eV and 150 eV. The observed increase of the MO peak intensity relative to that of the 5d VB is attributed to this cross-section effect. The Pt VB peak nearest the Fermi energy which is mainly t_{2g} in character, is found to decrease in intensity on adsorption of CO. In the present case synchrotron radiation in the $\hbar\omega > 100$ eV range appears to be especially valuable for studies of adsorbates.

*Based upon work in collaboration with P. S. Wehner, R. S. Williams, J. Stöhr, and D. A. Shirley and published in part in Solid State Commun. 20, 1141 (1976).

Photoemission studies of molecularly adsorbed gases on clean metal surfaces can provide unique insight into the adsorbate-substrate bonding. However, in order to obtain maximum information a careful choice of experimental conditions is necessary. Ideally, such studies should be carried out with an angle-resolved photoelectron energy analyzer on single-crystal substrates, using polarized radiation from a variable-energy photon source. It is also highly desirable to work in the photon energy range $\hbar\omega \sim 100$ eV, where surface sensitivity is maximal for most metals, so that substrate surface electronic structure is emphasized. With the availability of synchrotron radiation of energies up to 200 eV and beyond at the Stanford Synchrotron Radiation Laboratory, such experiments have now become feasible. Photoemission spectra studied as functions of photon energy yield valuable information on the characterization of the photoemission peaks[1] because the peak intensities (cross-sections) are determined by the orbital symmetries of the occupied states.[2] At the most favorable photon energies, angle-resolved studies can also yield information on the bonding symmetry.[3] The polarization of the synchrotron light should additionally enhance the expected angular effects.[3]

In this chapter we report photoemission studies of CO on Pt(111) using 40-150 eV synchrotron radiation. Our main goal was to assess the feasibility and value of photoemission experiments on an adsorbate-substrate system using variable photon energies above 100 eV.

A specific purpose of this study was to learn how the photoemission spectrum is modulated by cross-section effects and may be regarded as a

continuation of the previous study in Chapter II. Furthermore, it was intended to select an appropriate energy range for future angle-resolved studies. Accordingly two kinds of photoemission studies are reported below. First, we report measurements on the 5d VB of clean Pt in the energy range 40-200 eV. These studies were carried out at low resolution and are analyzed to yield the effective Pt 5d photoemission intensity as a function of photon energy. Secondly, the valence band region of a clean Pt(111) crystal and that of Pt(111) with CO adsorbed have been investigated in the energy range 40 eV $\leq \hbar\omega \leq$ 150 eV.

A high-purity single crystal of platinum with a (111) surface orientation was polished to 3-micron smoothness and etched repeatedly in a hot 3:1 solution of $HCl:HNO_3$ to remove the damage layer formed by polishing. Back-reflection Laue patterns taken to orient the crystals after this process showed sharp diffraction features, indicating the absence of a deep damage layer. The crystal was spot-welded to a thermally isolated rotatable mount.

Photoemission experiments were carried out at the 4° beam line of the Stanford Synchrotron Radiation Laboratory (SSRL)[4] using ultra-soft x-ray radiation emitted by the circulating electrons in the storage ring SPEAR. The monochromatic radiation was focused (image size $\sim$1×3mm) onto the Pt sample which was positioned in the focal point of a double-pass cylindrical-mirror energy analyzer (CMA).[5] A schematic diagram of the experimental geometry is shown in Fig. 1. The crystal orientation was adjusted for maximum photoemission intensity into the 360 acceptance cone of the CMA, operated in the retarding mode.[5]

The base pressure in the sample chamber was $\leq 1 \times 10^{-10}$ Torr. Since the crystal had been purged of bulk contamination in a previous experiment, cleaning of the surface required resistively heating the crystal to 910°C in 5×10^{-6} Torr oxygen for about 1 hour to remove residual carbon impurities. The sample was then flashed for 15 minutes to $\geq$ 1000°C to remove the adsorbed oxygen. During this period the sample chamber reached a maximum pressure of $\sim 8 \times 10^{-10}$ Torr with both a 220ℓ/sec ion pump and a 700ℓ/sec titanium sublimation pump in operation. After the sampled cooled and the pressure dropped below 3×10^{-10} Torr, the sample was again flashed to $\geq$ 1000°C for ~5 minutes. Procedures for cleaning Pt and the resulting PES spectra are shown in Chapter IV, Appendix A. All the photoemission studies were conducted at room temperature.

In the experiments designed to study the variation of Pt VB photoemission peak intensity with photon energy, spectra were recorded at a CMA pass energy of E_p = 100 eV, corresponding to a resolution of 1.6 eV. The Pt 5d-band intensity was defined as the area under the photoelectron energy distribution extending from the Fermi energy to about 7 eV binding energy (BE), corrected for inelastic scattering. The area was normalized with respect to the incident photon flux and the collecting efficiency of the CMA.[6] The resulting values for the Pt 5d intensities at photon energies ranging from 40-200 eV are shown in Fig. 2. The data points were collected during four beam periods (Runs 1-4 in Fig. 2) and the resulting energy dependence is shown as a solid line in the figure. The experimental error is estimated to be

approximately ±20%. As discussed in Chapter II the correction for the collecting efficiency of the CMA is somewhat uncertain. In deriving the dashed curve in Fig. 2 we have omitted the correction for the collecting efficiency; i.e., we have assumed that it is independent of the kinetic energy of the photoelectrons.

The variation of the Pt VB peak intensity is of interest because it is closely related to the energy dependence of the Pt 5d ionization cross-section. In fact, a direct proportionality between the VB intensity and its cross-section would exist in the limit of weak final-state band structure effects.[6] Whether or not such effects affect the observed spectrum depends on the type of experiments performed. For example, in angle-resolved photoemission from d-band metals dramatic changes in the shape of the spectra have been observed up to $h\omega = 200$ eV,[7] while for polycrystalline d-band metals final-state band structure effects appear to be weak above about 80 eV.[6,8] In the present case yet another experimental situation is encountered because only the total energy-integrated intensity of the spectrum rather than its detailed shape is of interest. It is apparent that this type of measurement is far less sensitive to final-state band structure effects than is an energy-resolved spectrum. We believe that the modulation of the Pt 5d intensity due to final-state effects does not exceed ±20% and thus lies within the experimental error bar for the solid curve in Fig. 2.

For the experiments with CO adsorbed on the Pt(111) surface, typical exposures of CO were 5L (1L = 1×10^{-6} Torr sec exposure) of research purity (99.99%) CO at 300°K. Exposures of 0.8L - 5L resulted

in equivalent spectra. After each exposure the pressure in the chamber returned immediately in the low 10^{-10} range.

As discussed by Gustafsson et al.,[1] the maximum in surface sensitivity is determined by both the energy-dependent photoemission cross-sections involved and the enhancement of the surface contribution at the energy where the electron escape depth is at a minimum. Our results for CO adsorbed on Pt reveal that there is a dramatic enhancement of CO spectral intensity relative to the Pt VB peak as a function of photon energy. Experimental results for clean Pt(111) and Pt(111) + 5L CO are displayed in Fig. 3 as solid and dashed curves, respectively. The spectra were recorded with a CMA energy resolution of 0.8 eV. Common features of all spectra are the two peaks at ∿8.7 eV (A) and ∿11.8 eV (B) binding energy (BE) relative to the Fermi level. We attribute A and B to the ($5\sigma + 1\pi$) and 4σ CO molecular orbitals respectively. Their BE's for the (111) Pt face agree with those obtained on polycrystalline Pt.[9] The CO spectral intensity relative to the Pt VB, while poor up to $h\omega \approx 70$-80 eV, is quite favorable at $h\omega = 150$ eV: in fact, better by a factor of three than at $h\omega = 40$ eV. The variation of ratio of the substrate and the adsorbate intensities with photon energy shown in Fig. 4 was derived in the following way. The experimental spectra (dashed curves in Fig. 3) were corrected for their inelastic backgrounds. The Pt 5d VB was defined over the range $E_f \leq BE \leq 7$ eV and its intensity was then compared to the area under the peaks B (4σ) and A ($5\sigma + 1\pi$).

We attribute this adsorbate intensity enhancement to the steep decrease in the Pt 5d intensity between 100 eV and 150 eV (the escape

depth probably varies by a factor of 2 or less, while the atomic cross-section varies by more than an order of magnitude). For comparison we have plotted in Fig. 5 the theoretical differential photoionization cross-section of the ($5\sigma + 1\pi$) molecular orbitals of CO as a function of incident photon energy[10] together with our experimental intensities for clean Pt as taken from Fig. 2. We realize the limitations of a planewave (PW) final state calculation for CO for quantitative comparison with experimental cross-sections. However, for lack of any more reliable theoretical or experimental results we have used the PW CO cross-sections shown in Fig. 5 to predict the ratio of the A ($5\sigma + 1\pi$) CO peak intensity relative to the Pt 5d VB intensity. The results, shown inserted on a linear scale in Fig. 5, are in good qualitative agreement with the experimental results in Fig. 4.

The above model can also account for the relative cross-sections of CO on Ni and Pd. Gustafsson et al.[1] found that the surface adsorbate signal falls off much more rapidly for CO on Ni than for CO on Pd. Ni is a 3d VB metal and as such should exhibit an increase in intensity to $h\omega \approx 120$ eV, then a more gradual monotonic decrease in intensity with increasing photon energy much like Cu.[8] For this case the CO spectral intensity falls off more rapidly than the Ni VB intensity, particularly for $h\omega < 120$ eV, giving a steep monotonic decrease of the surface adsorbate signal, relative to that of the substrate. On the other hand, Pd is a 4d VB metal with a radial node in the 4d wavefunction and as such should exhibit a Cooper minimum similar to the 4d VB of Ag.[6] The Ag intensity remains nearly constant for 40 eV $\leq h\omega \leq$ 80 eV,

then falls precipitously by over an order of magnitude to a minimum at $\hbar\omega \sim 140$ eV. The Pd 4d wavefunction should exhibit a similar pattern. We credit this Cooper minimum in the Pd VB intensity with the increase in relative adsorbate emission for Pd at $\hbar\omega > 80$ eV. The restriction of photon energy to $\hbar\omega \leq 100$ eV precludes Gustafsson et al. from observing the full extent of MO enhancement. Figure 6 compares the experimental data ($\hbar\omega \leq 100$ eV) of Gustafsson et al. for the ratios $\sigma_{CO}(1\pi + 5\sigma)/\sigma_{Ni}(3d)$ and $\sigma_{CO}(1\pi + 5\sigma)/\sigma_{Pd}(4d)$ with the ratios derived from Rabalais et al. theoretical CO cross-sections and our experimental intensities for clean Cu (3d) and Ag (4d). The data have been normalized at $\hbar\omega = 40$ eV. The agreement over the photon energy range 40-100 eV substantiates the qualitative arguments we have previously invoked. An extension of the calculated ratio for Ag and CO cross-sections allow us to predict enhanced CO/Pd ratio results for photon energies up to 150 eV, as shown in Fig. 7. Our results indicate that experiments with adsorbates such as CO adsorbed on either 4d or 5d VB substrates should benefit from synchrotron studies at high photon energies because of the selectivity for reducing substrate background intensity.

We feel that one other general observation about the spectra deserves comment. When CO chemisorbs on the (111) face of Pt, the valence band peak nearest the Fermi level always decreases in intensity relative to the other peaks in the Pt valence band.[11] Figure 8 shows the drop off of intensity at two different photon energies where the clean Pt and Pt+CO have been normalized with respect to photon flux. This seems to indicate that the states nearest the Fermi level are donating electrons to the CO molecule as it chemisorbs. The observation that the Pt

donates electrons to the CO molecule and not vice versa is supported by work-function measurements.[12] To determine the composition of the states nearest the Fermi level we have calculated the band structure of Pt using Smith's[13] parameterization of the Hodges, Ehrenreich, and Lang[14] tight-binding interpolation scheme. Figure 9 shows the calculated total valence band (VB) density of states and its decomposition into the t_{2g} and e_g components. The peak nearest the Fermi level is seen to arise in large measure (∿70%) from t_{2g} orbitals, which because of high surface sensitivity of the photoemission spectra at $h\omega$ = 70 eV and $h\omega$ = 150 eV, should mainly be located on surface Pt atoms.[15] Theoretical calculations by Desjonquères et al.[16] show that modification of the bulk bands at the surface does not change the basic t_{2g} character of the valence band near E_F. The dramatic decrease in the intensity of this peak on chemisorption of CO then indicates the involvement of surface t_{2g} orbitals in the chemisorption bond(s).

A further advantage to be gained by employing high photon energies between 130 eV and 1000 eV will be the use of the variation of photoelectric cross-section $\sigma(E)$ to determine molecular orbital character. The advantage afforded by making comparisons between UPS ($\leq$40 eV) and XPS (>1000 eV) spectra of free molecules has been expressed by W. C. Price.[17] The variations observed with photon energy in the UPS regime are well documented, but are not readily interpretable because of final-state effects. By using XPS photon energies of two widely different photon energies, however, it has been possible to observe different cross-section ratios within a given set of molecular orbitals. In this

region the deBroglie wavelength of the continuum electron in the final state becomes appreciably smaller than interatomic distances and the molecular orbital cross-sections become additive in their atomic constituents, in an LCAO/MO sense. It is well known that the 2s/2p atomic orbital cross-section ratio for second-row elements reverses dramatically from less than 1 at $\hbar\omega$ = 100 eV to about 10 for $\hbar\omega$ = 1000 eV. This has been demonstrated in molecules, for which ratios have been obtained with YMζ x-rays (132.3 eV)[2,18] and MgK$\alpha_{1,2}$ x-rays (1253.6 eV) and is in agreement with theory.[10] Similar effects should be applicable to the molecular orbitals of adsorbates. For approximately one monolayer detection of adsorbate MO's, MgKα x-rays have a photoemission cross-section too low for usefulness. With higher throughput monochromators in the energy range 150 eV $\leq \hbar\omega \leq$ 1500 eV synchrotron radiation experiments should yield the molecular orbital character of molecules adsorbed on a substrate.

The following chapter will demonstrate an alternative way to determine molecular orbital features, with the draw-back that detailed continuum final-state calculations are required.

REFERENCES

1. T. Gustafsson, E. W. Plummer, D. E. Eastman, and J. L. Freeouf, Solid State Commun. 17, 391 (1975).

2. M. S. Banna and D. A. Shirley, J. Electr. Spectrosc. and Related Phenomena 8, 23 (1976).

3. J. W. Gadzuk, Phys. Rev. B10, 5030 (1974); A. Liebsch, Phys. Rev. B13, 544 (1976).

4. H. Winick in Vacuum Ultraviolet Radiation Physics, edited by E. E. Koch, R. Haensel, and C. Kunz (Pergamon, Vieweg, 1974) p. 776; F. C. Brown, R. Z. Bachrach, S. B. M. Hagström, N. Lien, and C. H. Pruett, ibid, p. 785.

5. P. W. Palmberg, J. Electron Spectroscopy 5, 691 (1974).

6. P. S. Wehner, J. Stöhr, G. Apai, F. R. McFeely, R. S. Williams, and D. A. Shirley, Phys. Rev. B14, 2411 (1976).

7. J. Stöhr, G. Apai, P. S. Wehner, F. R. McFeely, R. S. Williams, and D. A. Shirley, Phys. Rev. B14, 5144 (1976).

8. See Chapter II.

9. P. R. Norton and P. J. Richards, Surface Sci. 49, 567 (1975) and G. Apai and P. S. Wehner, unpublished results.

10. J. W. Rabalais, T. P. Debies, J. L. Berkosky, J. J. Huang, and F. O. Ellison, J. Chem. Phys. 61, 516 (1974).

11. A similar observation was made by Norton and Richards (Ref. 9) for CO on polycrystalline Pt.

12. A. E. Morgan and G. Somorjai, J. Chem. Phys. 51, 3309 (1969).

13. N. V. Smith, Phys. Rev. B9, 1369 (1974). Smith's d-block parameters were used unchanged. The planewave (PW) and d-PW hybridization parameters were changed as follows: $\alpha = 0.014$, $V_{200} = 0.0082$, $V_{111} = -0.0071$, $B_1 = 0.4$, $B_2 = B_3 = 1.49$, $\beta = -0.06$ and a spin-orbit parameter $\xi = 0.038$ Ry.

14. L. Hodges, H. Ehrenreich, and N. D. Lang, Phys. Rev. 152, 505 (1966).

15. I. Lindau and W. E. Spicer, J. Electron Spectroscopy 3, 409 (1974).

16. M. C. Desjonquères and F. Cyrot-Lackmann, Solid State Commun. 18, 1127 (1976).

17. W. C. Price, A. W. Potts, and D. G. Streets, in Electron Spectroscopy, edited by D. A. Shirley (North-Holland, 1972) p. 187.

18. M. S. Banna and D. A. Shirley, J. Electron Spectroscopy 8, 255 (1976); M. S. Banna, Ph.D. Thesis, University of California, Lawrence Berkeley Laboratory Report, LBL-3473 (1974), unpublished.

FIGURE CAPTIONS

Fig. 1 *Experimental arrangement for photoemission studies. Electrons are analyzed by a cylindrical mirror analyzer (CMA).*

Fig. 2 Relative intensity of the Pt 5d VB as a function of photon energy. The dashed curve does not include a correction for the collecting efficiency of the CMA as is discussed in the text.

Fig. 3 Photoemission spectra of clean Pt(111) and Pt(111) + 5L CO in the energy range 40 eV $\leq \hbar\omega \leq$ 1 $\cup$ eV. Experimental resolution was 0.8 eV.

Fig. 4 *Intensity of the CO peaks B (4σ, 11.8 eV BE) and A (5σ + 1π, 8.7 eV BE) relative to the Pt 5d valence band intensity as a function of photon energy.*

Fig. 5 Plot of the theoretical CO (5σ + 1π) cross-section from Ref. 10 and the experimental Pt 5d VB intensity (Fig. 2). The resultant ratio is plotted as a function of photon energy in the insert on a linear scale.

Fig. 6 *The experimental results (Ref. 1) for the ratio of the CO peak (1π + 5σ) with respect to the Ni VB and Pd VB are compared with the ratio formed from the theoretical CO (1π + 5σ) cross-sections from Ref. 10 and our experimental cross-sections for Cu VB and Ag VB. Triangles represent the experimental data from Ref. 1. The solid curves represent the ratio formed from theory and our experiments.*

Fig. 7 The plots for Ag and CO cross-sections are used to predict enhancement of CO molecular orbitals on Pd at high photon energies.

Fig. 8 Photoemission spectrum of CO adsorbed on Pt(111) at $h\omega$ = 70 eV and 150 eV.

Fig. 9 Total valence band (VB) density of states and the t_{2g} and e_g projections for Pt 5d calculated in a tight-binding interpolation scheme as discussed in the text. The density of states histograms were convoluted with a Gaussian of FWHM = 0.5 eV.

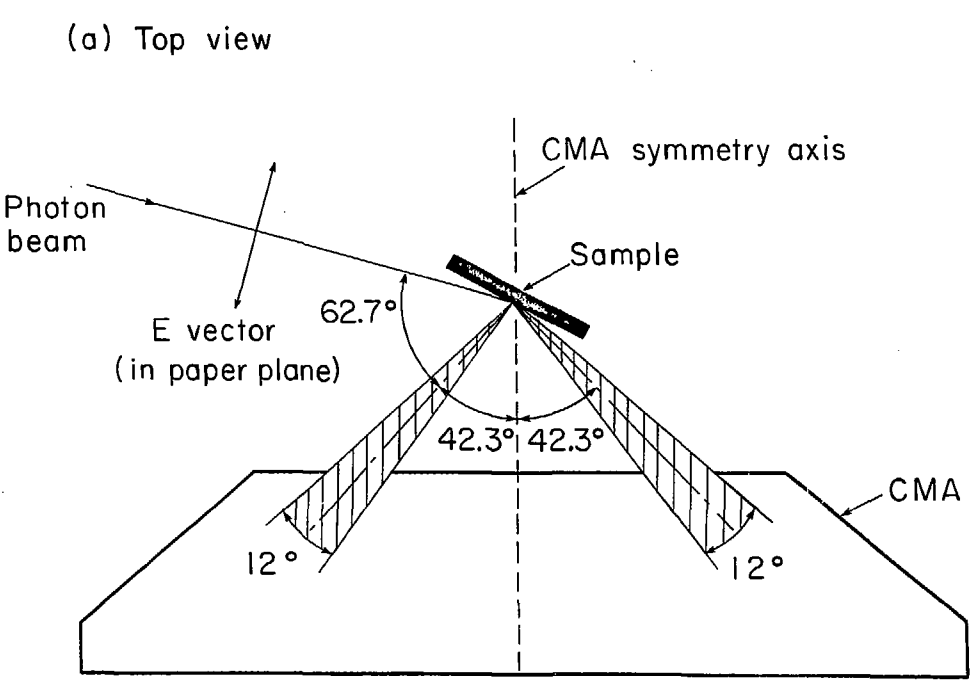

Fig. 1

XBL 764-2732

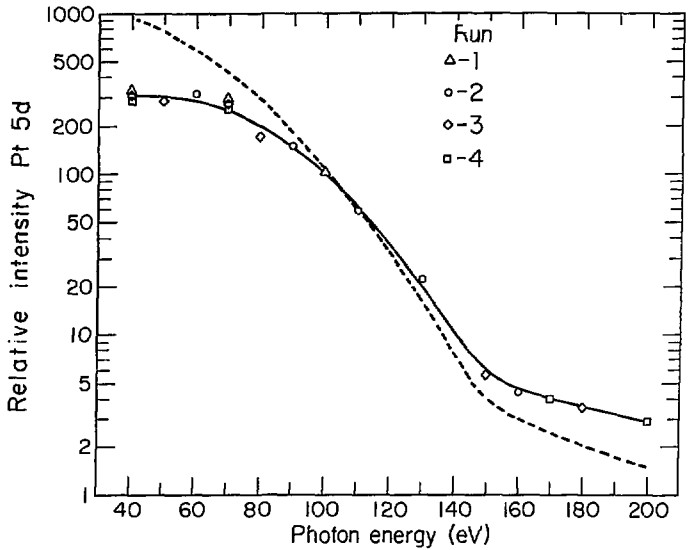

Fig. 2

XBL 764 2734

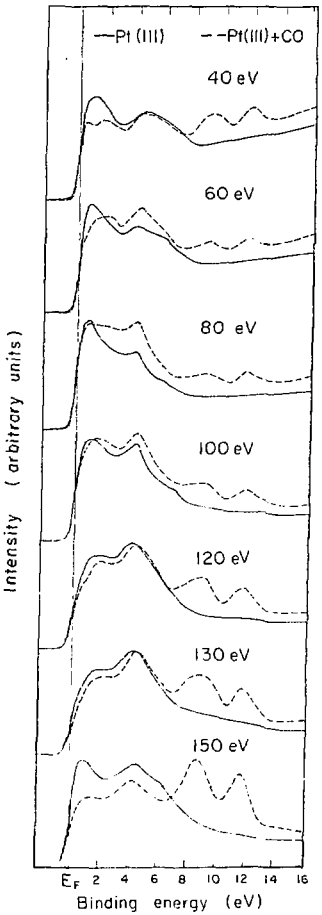
—Pt (111)
– –Pt(111)+CO
40 eV
60 eV
80 eV
100 eV
120 eV
130 eV
150 eV
Intensity (arbitrary units)
E_F 2 4 6 8 10 12 14 16
Binding energy (eV)

Fig. 3

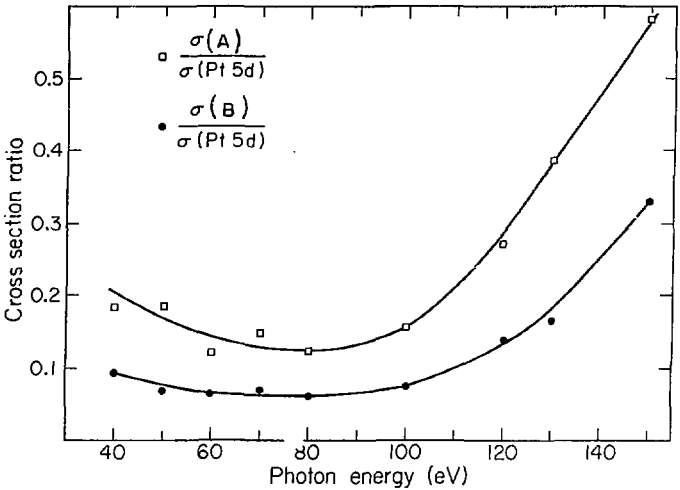

Fig. 4

XBL763-2370

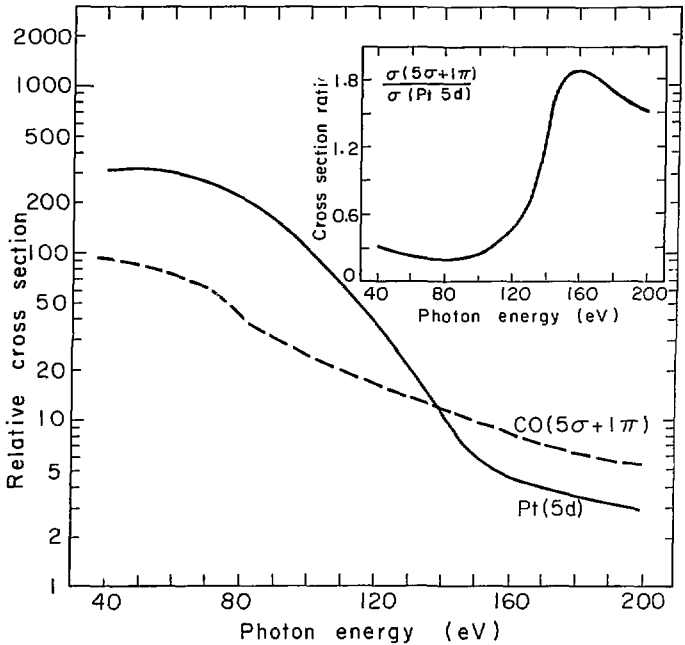

XBL 764-2786

Fig. 5

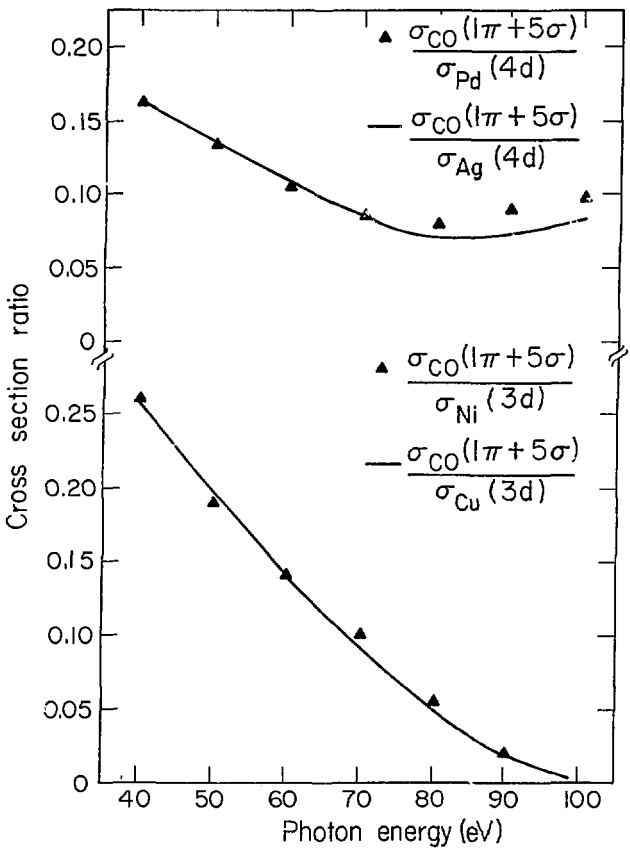

Fig. 6

XBL 775-1023

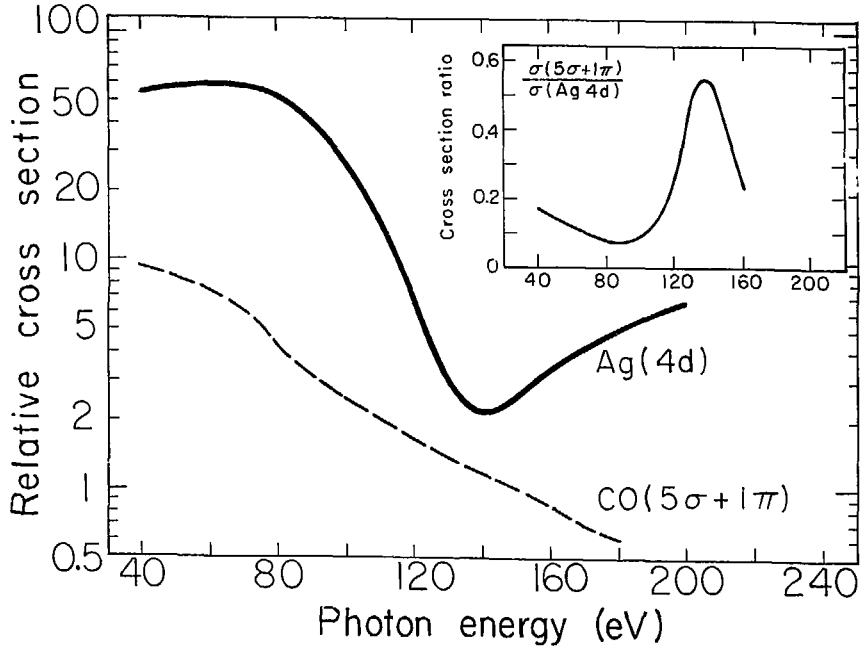

Fig. 7

XBL776-1114

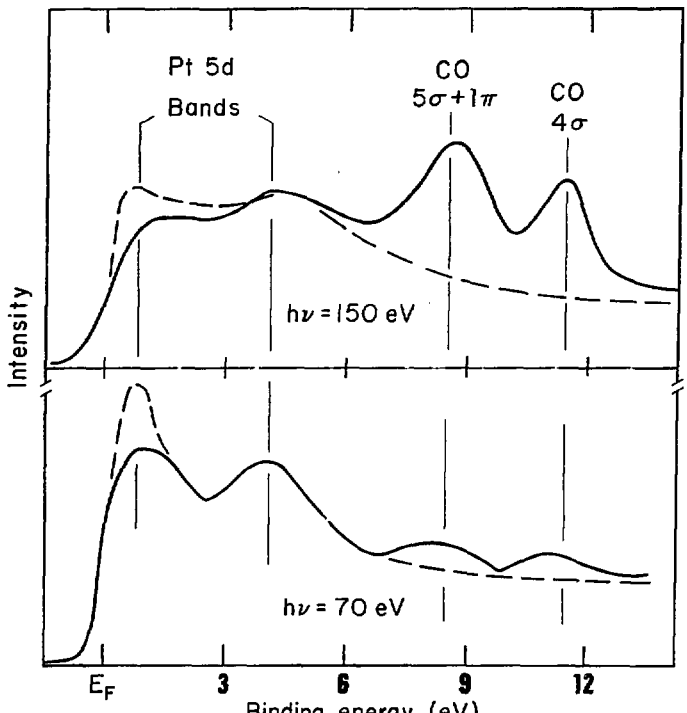

XBL 763-2485

Fig. 8

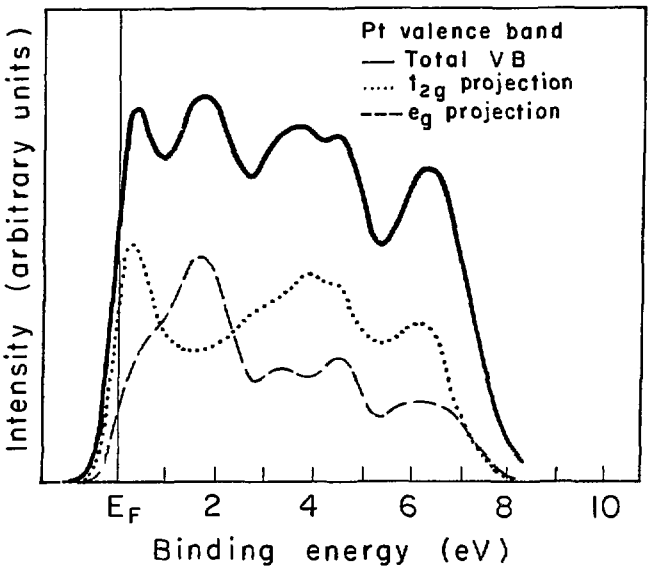

Fig. 9

XBL 764-2737

ANGLE-RESOLVED PHOTOEMISSION MEASUREMENTS

IV. ADSORBATE BONDING

A. Introduction

The photoelectron spectrum of an atomic or molecular species yields information about various ionic states. To a large degree the cross-section intensity for photoemission is dominated by the primary states which are directly related to Koopmans' description of photoionization[1] and can be described in terms of the ionization of an electron from a specific ground state orbital. However, Koopmans' frozen orbital ionic state does not represent a true many-electron eigenstate of the Hamiltonian; the electron density in the eigenstate actually has rearranged. The stabilization created by this relaxation[2] reduces the binding energy from that predicted by Koopmans' Theorem. By keeping the one-electron picture, relaxation can be visualized as a secondary process whereby the other electrons react to the hole created by the departing photoelectron.

For physisorbed species, the adsorbate photoemission peaks have the same structure that is observed from the free atom or molecule. However, the binding energy of each orbital is lowered relative to the gas-phase value by an additional relaxation energy originating from polarization of the substrate valence electrons to screen the adsorbate hole state. Both core-level and molecular orbital binding energies of adsorbed molecules are generally substantially smaller than the gas-phase values.

The molecular orbital peaks of chemisorbed molecules in photoemission spectra shift differently depending upon whether they are

involved directly in the chemical bonding to the surface. Demuth and Eastman[3] and Gustafsson et al.[4] found that most of the molecular orbitals of C_2H_2, C_2H_4, C_6H_6, and CO upon absorption on nickel shifted to lower binding energy. For the hydrocarbons the average shifts of all the σ orbitals were 3.2, 2.1, and 1.7 eV, respectively. In CO the 4σ and 1π orbitals shift by about 3.3 eV. Orbitals that form chemisorption bonds to the substrate tend to show the opposite behavior and shift to higher binding energy. This is attributed to an initial state effect. It has been observed for the least-bound π orbitals in C_2H_2, C_2H_4, C_6H_6 by Demuth and Eastman.[3] In CO a similar shift has been observed for the 5σ orbital, which merges with the 1π orbital, yielding a combined[4] The 5σ peak is the carbon "lone pair" orbital. The implication is that the carbon atom is bonded to the substrate and the CO molecule may be standing up as an adsorbate. Figure 1 illustrates the various changes which are expected in molecular photoemission spectra upon adsorption.

With the use of calculations to predict photoemission angular distributions from an oriented molecule in conjunction with angle-resolved PES measurements, it becomes possible to deduce the orientation of the molecule on a solid surface. Also there is the possibility of resolving the combined (1π + 5σ) peak of CO into a doublet.

B. The Orientation of CO on Pt(111) and Ni(111) Surfaces from Angle-Resolved Photoemission*

ABSTRACT

Angle-resolved photoemission spectra of the molecular orbitals of chemisorbed CO on Pt(111) and Ni(111) substrates show a strong angular variation of the peak intensity ratio. Comparison with Davenport's Xα calculations establishes that CO stands up on these substrates with the carbon atom bonded to the substrate. The Pt 5d (t_{2g}) orbitals are also verified to be strongly involved in chemisorption bonding to CO. Angular measurements have separated the combined ($1\pi + 5\sigma$) peak into a doublet and indicate that the MO assignment in the chemisorbed CO is different than the gas-phase MO ordering.

*Work performed in collaboration with P. S. Wehner, J. Stöhr, R. S. Williams, and D. A. Shirley and published in part in Phys. Rev. Lett. 37, 1497 (1976).

The interaction of chemisorbed adsorbate molecules with catalytically active substrates has formed the focus of much recent research activity in surface physics. Because of the importance of the CO/Pt and CO/Ni systems in heterogeneous catalysis for synthesis of hydrocarbons, these systems have served as prototypes for surface studies. Until this experimental study however, no firm evidence had been presented regarding the orientation of adsorbate CO molecules on crystalline nickel or platinum surfaces.

Davenport[5] presented SW Xα calculations of photoelectron angular distributions from the molecular orbitals of oriented (gas phase) CO molecules and pointed out that chemisorbed CO should display similar angular distributions provided that the molecular wavefunctions are not strongly perturbed by the substrate. In this chapter we report photoelectron angular distributions from CO adsorbed on both Pt(111) and Ni(111) surfaces. These data provide definitive evidence that the CO molecules "stand up" in both cases, with the carbon atoms bonded to the substrate. Furthermore, the spectra clearly show that the t_{2g} orbitals of the Pt 5d band are strongly involved in the Pt-C chemisorption bond. The experiments reported here were carried out with conventional photoemission equipment (He lamp, cylindrical mirror analyzer) and thus point out the potential of such studies to determine bonding geometries. It is clear that by making use of variable-energy, highly-polarized synchrotron radiation such studies become even more powerful.

Experiments were carried out using the $\hbar\omega$ = 40.8 eV radiation emitted by a He II resonance lamp. Single crystals of Pt and Ni were

cut along the (111) planes and cleaned in situ under ultra-high vacuum conditions. In the case of Pt it was necessary to alternate periods of Ar^+ bombardment of the specimen at 950°C and oxidation in an atmosphere of 10^{-5} Torr O_2 at 850°C for two weeks in order to remove calcium and carbon impurities diffusing to the crystal surface from the bulk. Nickel was cleaned by repeated Ar^+ bombardment and annealing. (See Appendix A). The photoemission studies were conducted at a background pressure of impurities (other than He) of $< 8 \times 10^{-11}$ Torr. Differential pumping was such as to allow a background He pressure of $\sim 1 \times 10^{-9}$ Torr. In the angle-dependent studies both the unpolarized photon beam and the propagation direction of the analyzed electrons were in a horizontal plane, and the crystal could be rotated about a vertical axis in the plane of the (111) surface. Angle-resolved photoemission (ARP) was facilitated by masking all but an 11° arc of a cylindrical mirror analyzer.[6,7] The geometrical arrangement of the slit is shown in Fig. 2(b). The effective acceptance area of the CMA is defined by the ±6° acceptance width of the CMA[8] and by the ±5.5° slit width of the shield yielding an angular resolution of ±6° in the horizontal and ±4° in the vertical plane (cf. Fig. 2). It was found that the shield reduces the counting efficiency of the CMA by approximately 360°/11°, as expected. Figure 3 shows the variation of the clean valence-band spectra (solid line) and corresponding spectra after adsorption of ~4L CO (dotted line), plotted against θ, the angle of rotation from the crystal normal to the photoelectron $\vec{q}$ direction, for both crystals. The spectra shown in Fig. 3 were recorded with an experimental resolution of ~0.2 eV.

The CO molecular orbitals labeled A and B in Fig. 3 are manifest as two peaks falling at ∿8.1 and ∿10.8 eV binding energy below the Fermi level (E_F) in Ni and at ∿9.2 and ∿11.7 eV in Pt, respectively. The higher binding energy (BE) peak (B) has been assigned to the 4σ orbital of CO, while the lower BE peak (A) is attributed to a combination of the 1π and 5σ orbitals.[4] In both cases the two peaks are of nearly equal intensity for $\vec{q}$ near the surface normal, with the B/A ratio decreasing as $\vec{q}$ is rotated toward the crystal surface. In Fig. 4(c) we have plotted the intensity ratio I_B/I_A of the two molecular orbitals (MO's) A and B for the case of CO on Ni(111) and CO on Pt(111) as a function of the angle (θ) between the surface normal and photoelectron propagation direction. The details of the crystalline orientation with respect to the photon beam and the detector are shown in Figs. 4(a) and 4(b). In Fig. 4(d) we have plotted the angular dependence of the ratio $4\sigma/(1\pi + 5\sigma)$ calculated from Davenport's angular distribution, for three orientations of the CO molecule with respect to the surface. The calculations have been scaled for the best fit to the experimental curves. We believe this is justified because Davenport's calculation does not predict the correct magnitude for the total cross-section of the 1π and the 4σ orbitals at $\hbar\omega \approx 41$ eV (see Fig. 2, Ref. 5). For this reason we compare our results only to the angular dependence of the ratio and not the absolute magnitude.

In our calculation, we take the unpolarized incident radiation to be composed of two orthogonal linearly polarized components one of which is in the plane containing the incoming photon beam and the detector and the other which is perpendicular to this plane ($\vec{A} = \vec{A}_{\parallel} + \vec{A}_{\perp}$).

Because for unpolarized light the two components $\vec{A}_{\parallel}$ and $\vec{A}_{\perp}$ are incoherent the photoexcitation matrix element can be written

$$\int_0^{2\pi} |< f|\vec{A} \cdot \vec{p}|i >|^2 d\alpha \sim |< f|\vec{A}_{\parallel} \cdot \vec{p}|i >|^2 + |< f|\vec{A}_{\perp} \cdot \vec{p}|i >|^2 \quad . \tag{1}$$

The contributions from the two components to the differential photoemission cross section were calculated according to the following analytical expression[9]

$$\frac{d\sigma}{d\Omega} = A(\Theta)\cos^2\Theta_A + \left(B(\Theta) + C(\Theta)\cos 2\phi\right)\sin^2\Theta_A + D(\Theta)\sin\phi\sin\Theta_A\cos\Theta_A \quad , \tag{2}$$

where Θ_A is the polar angle of $\vec{A}_{\parallel}$ or $\vec{A}_{\perp}$, respectively, and Θ and ϕ are the usual polar and azimuthal angles of photoemission with respect to the CO axis of the oriented molecule.[5]

Comparison of the experimental intensity ratio I_B/I_A for the adsorbate-substrate systems (Fig. 4(c)) with the scaled theoretical intensity ratio $4\sigma/(1\pi + 5\sigma)$ for an oriented CO molecule (Fig. 4(d)) strongly favors the configuration where CO stands up, with the C bonded to the substrate. Note in particular that the configuration with O bonded to the substrate can be excluded because the $4\sigma/(1\pi + 5\sigma)$ ratio vanishes for angles $\Theta \geq 20°$. The overall good agreement between the experimental curves in Fig. 4(c) and the solid curve in Fig. 4(d) is not expected to be perfect in detail, mainly because the 5σ orbital is expected to be somewhat perturbed through its interaction with the substrate.[10] We feel that the present results, besides determining the orientation of CO on Ni(111) and Pt(111), also prove in general that angle-resolved

ultraviolet photoemission can be used to determine bonding geometries. One other point which needs to be discussed is the different behavior of the ratio I_B/I_A with Θ for CO on Ni(111) and CO on Pt(111). This may be due to a difference in the detailed nature of the adsorbate-substrate bonding for the two systems resulting in initial[11] and/or final[12] state effects which determine the photoemission angular distributions.

Although CO orientation has been determined, the precise compositional structure with energy for the MO levels nearest the Fermi level has not been resolved. Subsequent experiments with a different incident photon beam direction, hence, a change in the relationship between polarization and the electron emission angle, have allowed the ($1\pi + 5\sigma$) peak to be resolved into a doublet. The change in geometry can be seen in Fig. 5 (cf. Fig. 2). Now, the photon beam from the He lamp enters from a different port in the UHV chamber forming an angle with respect to the CMA axis of 77.7° rather than 105.0° as employed previously. The analyzer mask has also been rotated 180°. Comparison of the Pt(111) + CO data in Fig. 6 with data in Fig. 3 reveals that several features are significantly different. At a photoelectron propagation angle normal to the surface (Θ = 0°) the composite peak nearest E_F is more intense than the high binding energy MO, when compared to the former data. Also as the angle (Θ) between the surface normal and photoelectron propagation direction increases, the low BE MO splits into a double whereas the former data revealed only a slight increase in asymmetry.

Calculation of the differential photoemission cross-section for the orbitals using equation (2) favors 1π orbital intensity at high Θ angles (i.e., low take-off angles to the surface). In the former geometry the 1π orbital intensity was also favored at high Θ angles, however it appears only as an asymmetric broadening (cf. Fig. 3). There have been several published experiments which have also resolved the low BE peaks of CO into a doublet.[13-15] Comparison with these data is not possible since the substrates and crystal face orientations are different. What is apparent is that the MO's of CO may reorder with respect to the gas-phase molecul. depending on the particular substrate. Williams et al.[13] studied a saturation coverage of CO on Ni(111) and concluded, on the basis of symmetry arguments (one of the orbitals within the doublet peak revealed a similar intensity profile to the 4σ level), that the 1π level was nearest the Fermi level. Davenport's calculations[16] of the relative angular distributions for William's experiments also support this assignment. The calculated 5σ level intensity was found to be too low, however that may be expected for chemisorbed CO due to an admixture of metal electron density into the bonding orbital. Our results also show a high intensity for the orbital we assign to the 5σ level and we believe that this additional metal orbital intensity is responsible.

Recent theoretical calculations by Batra and Bagus[10] and Bagus and Hermann[17] also indicate that the ordering of the CO molecular orbitals 5σ and 1π are reversed upon chemisorption. Batra and Bagus utilized a model cluster with CO and five nickel atoms to calculate

the electronic structure using the spin-unrestricted SCF-Xα-SW method. The calculation was performed by the transition state method and included relaxation effects. The second calculation by Bagus and Hermann was an ab initio Hartree-Fock calculation for a linear NiCO moiety which obtained wavefunctions and energies of the relaxed final ionization states as well as for the initial states. Each calculation indicates that bonding of CO to nickel involves metal s, p, and d orbitals. The most highly perturbed orbital is the 5σ state which was found to contain ~13% Ni 3d character for linear NiCO. The large cluster calculations also indicate that there are electronic charge rearrangements in the substrate which alter the substrate density of states. Figure 7 reveals in a more dramatic way than previously the attenuation of valence band states near the Fermi level with CO chemisorbed on Pt(111). It is apparent when comparing this figure with Fig. 8 in Chapter III that angle-resolved photoemission can be more sensitive to electronic structure changes in the substrate than angle-integrated PES.

APPENDIX A

Single crystals have been cut from rods which have been zone-refined to yield low impurity concentrations. Nevertheless these bulk impurities may diffuse to the crystal surface and be responsible for altering the surface, both in structure and chemical reactivity. Common impurities in platinum samples are carbon, calcium, phosphorus, and sulfur. Nickel samples contain sulfur as their major contaminants. Single crystals were prepared by orienting with a Laue back-reflection x-ray technique, spark cutting an approximately 1mm thick slice with the proper crystallographic orientation, polishing the face ($\sim$0.5μ finish), and etching to remove surface induced strain.

After identification of surface contaminants had been made by either Auger electron spectroscopy (AES) or x-ray photoelectron spectroscopy (XPS) their removal was accomplished by a series of oxidation, Ar^+ bombardment, and heat treatments, as mentioned in the text. We have found that the rate limiting step for the removal of impurities is their diffusion to the surface. This diffusion process is also an extremely sensitive function of temperature. Figure 8 reveals the sensitivity of UPS for monitoring impurity migration to the surface. Spectrum A at T = 25°C represents the PES for a partially clean Pt(111) surface. Up to T = 1000°C (B) there is diffusion of impurities to the surface affecting the spectrum, especially at BE $\sim$5-10 eV. By 1200°C (C) the surface impurities have diffused back into the bulk and a substantially clean Pt(111) surface is obtained. Cooling the sample back down to 1000°C reprecipitates the impurities at the surface in a concentration sufficient enough to mask any rise at the Fermi level.

REFERENCES

1. T. Koopmans, Physica 1, 104 (1933).

2. The difference in binding energy between the Koopmans' Theorem value and experimental observation is called the relaxation energy.

3. J. E. Demuth and D. E. Eastman, Phys. Rev. Lett. 32, 1123 (1974).

4. T. Gustafsson, E. W. Plummer, D. E. Eastman, and J. L. Freeouf, Solid State Commun. 17, 391 (1975).

5. J. W. Davenport, Phys. Rev. Lett. 36, 945 (1976).

6. P. W. Palmberg, J. Electron Spectrosc. 5, 691 (1974).

7. H. Niehus and E. Bauer, Rev. Sci. Instrum. 46, 1275 (1975). It should be noted that the CMA used in our study (Physical Electronics) does not accept electrons equally into its 360° acceptance cone. There are posts in four (1:30, 4:30, 7:30, and 10:30 o'clock) positions inside the analyzer which block the electrons along the respective trajectories. This fact has to be considered when rotating the slit for angle-resolved studies as proposed in the above reference. In our case the slit was fixed in the 3 o'clock position and hence the posts had no effect on our measurements.

8. The value $\Delta\alpha = 6°$ for the acceptance angle of the CMA quoted in Ref. 6 (footnote Fig. 2) is incorrect and should read $\Delta\alpha = 12°$ or $\alpha = (42.3\pm6)°$.

9. J. W. Davenport (private communication) supplied the analytical expression for the cross-section and calculated values for $A(\Theta)$, $B(\Theta)$, $C(\Theta)$, and $D(\Theta)$. In the case for the CO molecule lying down on the surface we have assumed a random orientation.

10. I, P. Batra and P. S. Bagus, Solid State Commun. 16, 1097 (1975).

11. J. W. Gadzuk, Phys. Rev. B10, 5030 (1974).

12. A. Liebsch, Phys. Rev. B13, 544 (1976).

13. P. M. Williams, P. Butcher, J. Wood, and K. Jacobi, Phys. Rev. B14, 3215 (1976).

14. D. R. Lloyd, C. M. Quinn, and N. V. Richardson, Solid State Commun. 20, 409 (1976).

15. G. Broden and T. N. Rhodin, Solid State Commun. 18, 105 (1976).

16. J. W. Davenport, Ph.D. Thesis, University of Pennsylvania, 1976.

17. P. S. Bagus and K. Hermann, Surface Science (to be published).

FIGURE CAPTIONS

Fig. 1 Energy level diagram for photoemission from an adsorbate molecule, showing ground state M, core-hole state M^+ (c), and hole states M^+(VBS) and M^+(VNBS) of valence orbitals that do and do not bond to the substrate, respectively. Vacuum reference levels are used. Hole state energies, i.e., binding energies, are lowered on physisorption because of screening by the substrate's valence electrons. The core-hole relaxation energy ΔE_{RC} is greater than that of the valence-level hole states, ΔE_{RV}. On chemisorption, the adsorbate-to-substrate bonding orbital is identified by an increase in its hole-state (binding) energy, ΔE_{BOND}.

Fig. 2 Experimental geometry for angle-resolved photoemission studies. A cylindrical-mirror analyzer (CMA) is modified by means of a slit aperture (shield) to allow angle-resolved measurements. The effective angular resolution is ±6° in the horizontal and ±4° in the vertical plane.

Fig. 3 Photoemission spectra of clean Ni(111) and Pt(111) (solid lines) and Ni(111) + 4L CO and Pt(111) + 4L CO (dotted lines) at $\hbar\omega$ = 40.8 eV as a function of the angle θ between the surface normal and the photoelectron propagation direction. θ is defined in Fig. 4(a).

Fig. 4 (a) Experimental arrangement of the photon beam and detector with respect to the crystal normal. θ is defined positive for clockwise rotation, negative for counterclockwise rotation of the crystal normal with respect to the fixed photoelectron

propagation direction into the analyzer.

(b) Experimental orientation of the crystals in the (111) plane.

(c) Intensity ratio I_B/I_A of the molecular orbital peaks A and B in Fig. 3 as a function of Θ, where Θ is defined in Fig. 4(a).

(d) Calculated intensity ratio $4\sigma/(1\pi + 5\sigma)$, scaled to best fit experiment, for three orientations of the CO molecule with respect to the surface as a function of Θ, where Θ is defined in Fig. 4(a).

Fig. 5 Alternate experimental geometry for angular resolved photoemission studies. A different entrance port for the He II radiation has been used and the slit aperture has been rotated 180° from the previous geometry shown in Fig. 2.

Fig. 6 Photoemission spectra of Pt(111) + 4L CO at $h\omega$ = 40.8 eV as a function of the angle Θ between the surface normal and the photoelectron propagation direction. An increase in Θ represents a counterclockwise rotation of the sample in Fig. 5.

Fig. 7 Angle-resolved photoemission spectra of clean Pt(111) and Pt(111) + 4L CO at Θ = 40°.

Fig. 8 Temperature dependence spectra of a Pt(111) crystal surface showing the diffusion of bulk impurities to the surface. At temperatures up to T = 1000°C impurities are found to diffuse to the surface. By T = 1200°C surface impurities appear to diffuse back into the bulk.

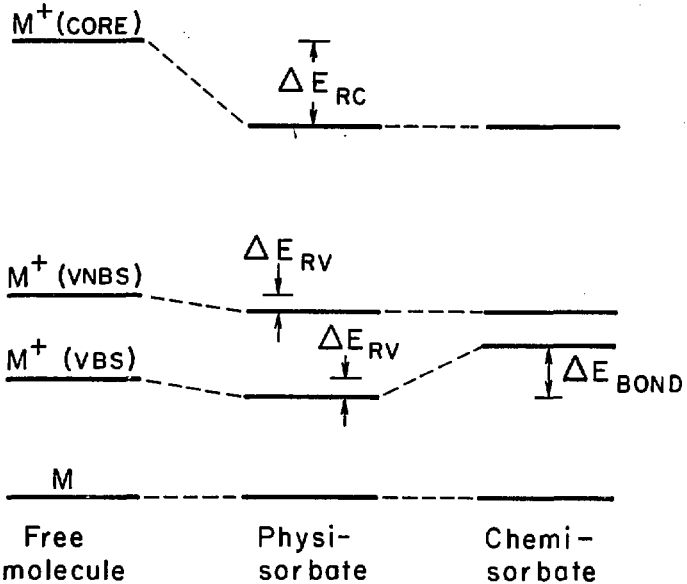

Fig. 1 XBL751-2142

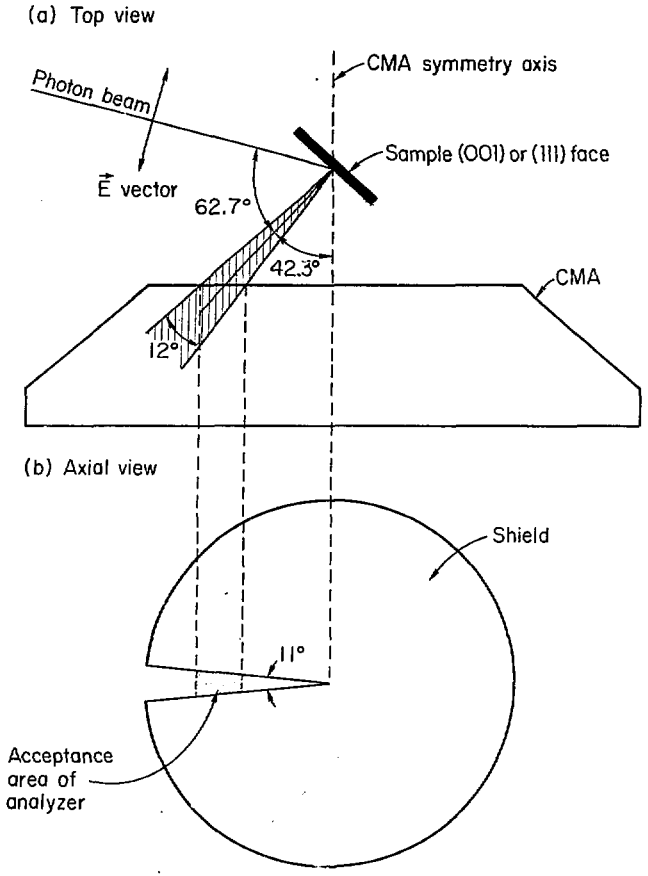
(a) Top view
CMA symmetry axis
Photon beam
Sample (001) or (111) face
$\vec{E}$ vector
62.7°
42.3°
CMA
12°
(b) Axial view
Shield
11°
Acceptance
area of
analyzer
XBL 763 2443

Fig. 2

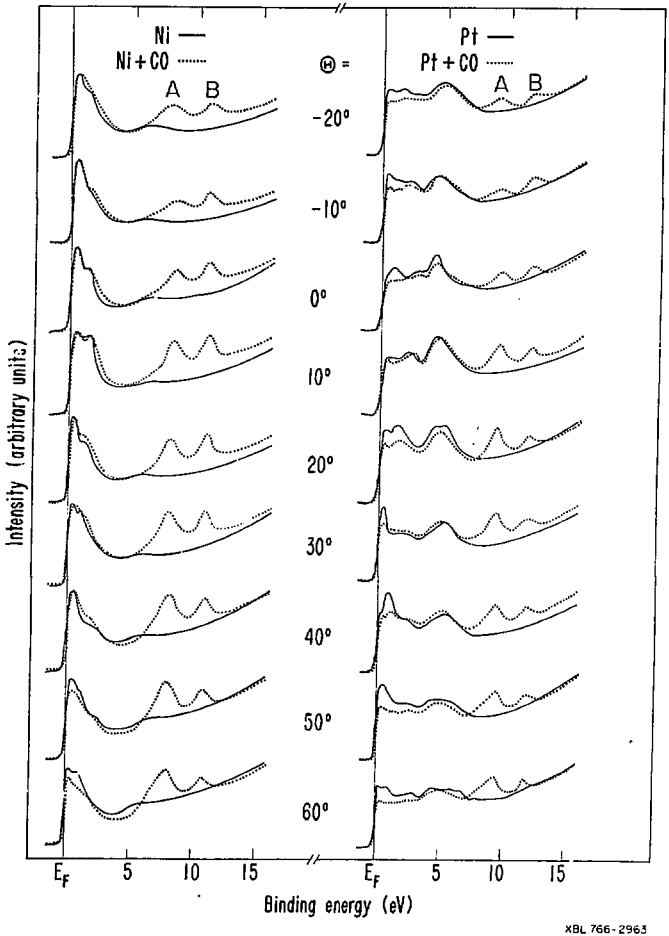

XBL 766-2963

Fig. 3

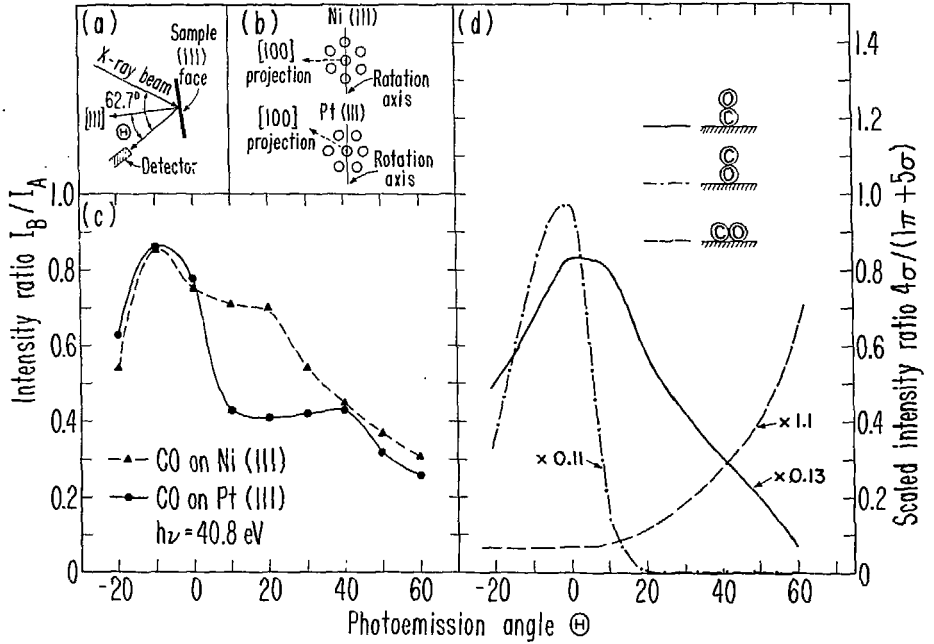

Fig. 4

XBL769-3919

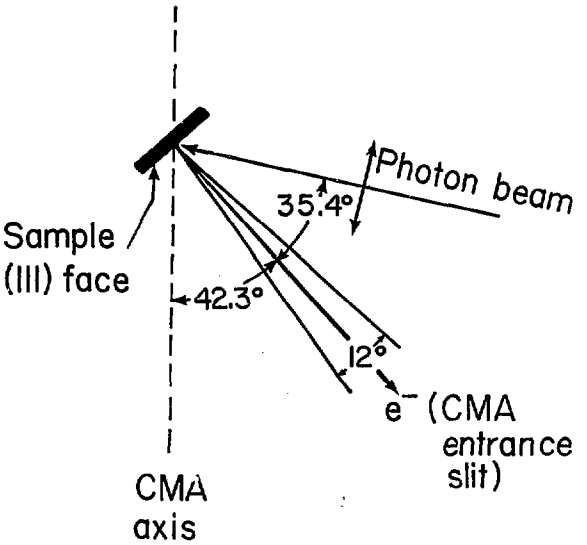

XBL775-1017

Fig. 5

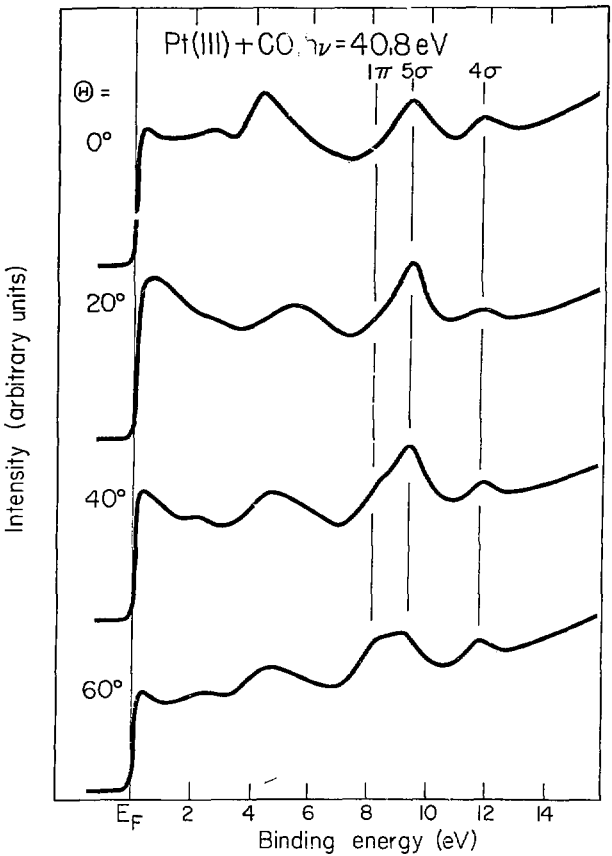

Fig. 5

XBL 775-1018

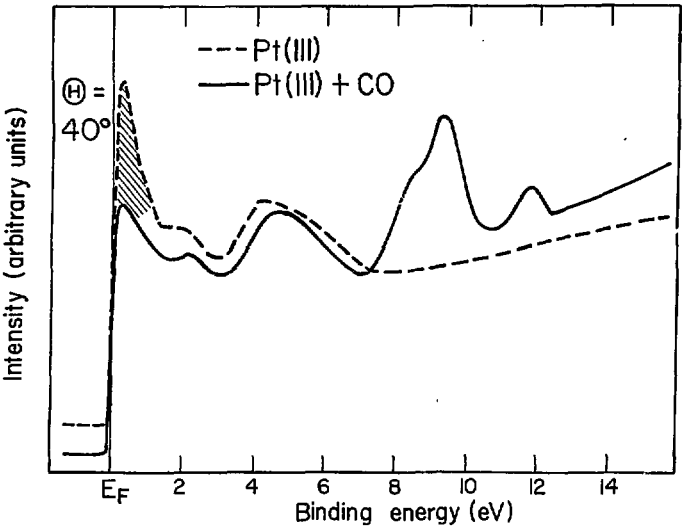

XBL 775-1021

Fig. 7

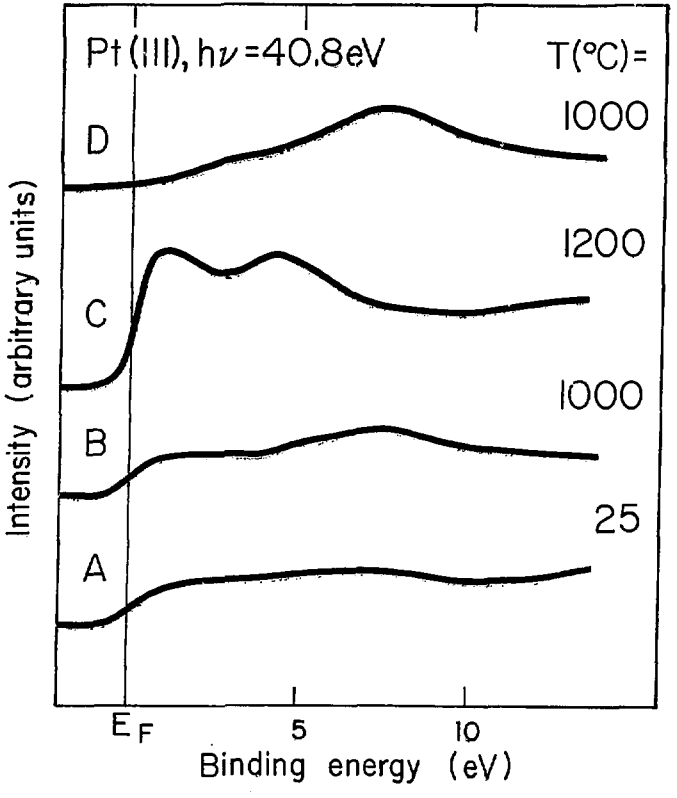

Fig. 8

XBL 775-1024

V. ANGLE AND ENERGY DEPENDENT PHOTOEMISSION FROM CO ON Pt(111)

Low-energy electron diffraction has been the technique of choice to determine surface crystallographic structure.[1] In this technique a monoenergetic beam of electrons within the energy range of several tens of electron volts to several hundred electron volts impinges on a periodic crystal and the coherent elastically back-scattered electrons form diffraction patterns because their wavelengths are comparable to that of lattice spacings. Since electrons within this energy regime exhibit strong electron-solid interactions, the scattering occurs mainly from the surface region. The analysis of the scattered intensities has been most complicated because of the strong multiple scattering. For the study of adsorbed molecules LEED analysis has been hampered by damage and dissociation of the molecule by the electron beam.[2] Electrons tend to be more damaging than photons because they have high probabilities per incident particle of a valence electron excitation, the beams have a greater flux, and the radiation is concentrated nearer the surface with a high degree of collimation.[1] In addition LEED scattering requires ordered domains $\sim$500Å in diameter because of experimental limitations with the coherence width of the electron beam.

Photoemission techniques perhaps offer an alternative way to determine site symmetry and atomic positions of adsorbed atoms and molecules on solid surfaces. A photoelectron from a given initial state can make its way to the detector either directly or by scattering from the atoms of the solid. Figure 1 indicates the two processes schematically. Process 1 represents directional photoemission from within

the molecule, including its final-state interference effects. Process 2 is due to scattering from atoms other than those within the molecule. By analyzing the angular distributions, both at electron energies where the electrons come primarily from the directional photoemission process within the molecule and at electron energies where a major portion of intensity backscatters from the substrate, a deconvolution of the effects may yield coordinations of the chemisorption bond and geometry of bonding sites. The theory of these low energy electron diffraction effects in the photoemission process have already been outlined by Liebsch[3] and Tong and Van Hove.[4] The advantage of employing photoemission from localized atomic or molecular orbitals is that the technique is applicable to isolated adsorbate units and does not require a periodic-adsorbate system as LEED does. Both LEED and photoelectric LEED still require highly ordered single crystal surfaces. By employing a variable photon energy source and a single crystal substrate, angle-resolved studies appear to provide strong evidence for electron scattering processes.

Several angle-resolved photoemission spectra for Pt(111) + 4L CO are shown in Fig. 2. Common features of all spectra are the two peaks at $\sim$9.2 eV (A) and $\sim$11.8 eV (B). Peaks A and B are assigned to the ($1\pi + 5\sigma$) and 4σ CO molecular orbitals, respectively. Figure 2 also reveals that the angular-resolved photoemission spectra of the molecular orbitals (MO's) of chemisorbed CO on a Pt(111) substrate show a strong angular variation of the peak intensity ratio B/A, as θ, the angle between the crystal normal and the photoelectron propagation direction, is changed. The experimental results at $h\omega = 40$ eV, using

both unpolarized (He II) and polarized (synchrotron) radiation, fit the calculated ratio $4\sigma/(1\pi + 5\sigma)$ for an oriented CO molecule[5] which stands up on the substrate with the carbon atom bonded to the substrate. Details of the crystalline orientation with respect to the photon beam and the detector are shown in Figs. 3(b) and 3(c). In Fig. 3(a) the angular dependence of the ratio $4\sigma/(1\pi + 5\sigma)$ is plotted for unpolarized ($\hbar\omega$ = 40.8 eV) radiation as well as for polarized synchrotron radiation at $\hbar\omega$ = 40 eV and $\hbar\omega$ = 150 eV. The polarization of the synchrotron radiation enhances the angular dependence of the spectra, as seen for $\hbar\omega$ = 40 eV. At $\hbar\omega$ = 150 eV the molecular orbitals of CO are more intense with respect to the valence band (VB) than at $\hbar\omega$ = 40 eV, as we discussed in Chapter III. Also there is a dramatic reversal in the angular variation of relative MO peak intensities. Since the SW-$X\alpha$ calculations of Davenport[5] at $\hbar\omega$ = 40 eV are in qualitative agreement with a planewave final state picture, a similar behavior for $\hbar\omega$ = 40 eV and $\hbar\omega$ = 150 eV spectra is expected on the basis that the photoelectron continuum state should be more planewave-like at higher energies, contrary to our experimental results.

There are two factors, however, which may influence the angular distributions: (1) intramolecular scattering and (2) backscattering from the substrate. Figures 4 and 5 show the relative peak intensities and the ratio $4\sigma/(1\pi + 5\sigma)$ for normal photoemission and for a 45° electron take-off angle. Spectra were normalized to the transmission of the monochromator as measured with an Al_2O_3 photodiode.[6] Peak intensity modulations for the 4σ and $(1\pi + 5\sigma)$ peaks are found to be much more

pronounced for normal photoemission than for comparable spectra taken at a 45° electron take-off angle. The enhanced modulations in the normal direction may represent scattering resonances within the CO molecule; if so, these resonances for normal electron emission would be strong indicators that the molecular axis is perpendicular to the Pt substrate surface, since one would expect resonances to be most pronounced along the CO internuclear axis. Another possible origin lies in final state interference effects between the primary photoelectron-wave and backscattered wave from the substrate.[3] This effect is expected to become more important at higher (~100 eV) kinetic energies of the photoelectron.[4] We note that such interference effects, if shown to be important, can yield information on the geometry of the adsorbate-substrate complex. We hope that the results presented in this chaper will stimulate theoretical calculations extending to higher photon energies.

REFERENCES

1. C. B. Duke in Advances in Chemical Physics, Vol. XXVII, edited by I. Prigogine and S. A. Rice (Interscience).

2. J. C. Tracy, Journal of Chem. Phys. 56, 2736 (1972).

3. A. Liebsch, Phys. Rev. Lett. 32, 1203 (1974); A. Liebsch, Phys. Rev. B15, 544 (1976).

4. S. Y. Tong and M. A. Van Hove, Solid State Commun. 19, 543 (1976) and references therein.

5. J. W. Davenport, Phys. Rev. Lett. 36, 945 (1976).

6. W. Gudat, C. Kunz, and W. Lenth in Proceedings of the Fourth International Conference on Vacuum Ultraviolet Radiation Physics, Hamburg, July 1974, edited by E. Koch, R. Haensel, and C. Kunz (Pergamon, Vieweg, 1974). See Chapter I for calibration details.

FIGURE CAPTIONS

Fig. 1 Illustration of two processes which may contribute to the photoemission process: (1) photoelectrons originating from the molecule and making a direct path to the detector, and (2) indirect emission after backscattering from the substrate.

Fig. 2 Comparison of experimental spectra of CO on Pt(111) using 150 eV and 40 eV synchrotron radiation and 40.8 eV He II radiation as a function of the photoemission angle, θ as defined in Fig. 3b. Note the strong variation in the CO peak intensity of A and B with a change in angle or photon energy.

Fig. 3 Plot of the measured intensity ratio I_B/I_A (compare with Fig. 2) for two different light sources (He II and synchrotron) and photon energies (~40 eV and 150 eV). All spectra were taken in the same geometry as shown in Figs. 3b and 3c. The difference between the intensity ratio derived from He II and synchrotron radiation spectra is due to the polarized nature of the synchrotron light. The dramatic inversion of the ratio I_B/I_A between 40 eV and 150 eV may indicate the importance of final-state scattering effects.

Fig. 4 Integrated intensity from CO ($1\pi + 5\sigma$) and CO 4σ adsorbate MO levels as a function of photon energy. The geometry is the same as described in Figs. 3b and 3c. The right hand panel shows the ratio for $4\sigma/(1\pi + 5\sigma)$ as a function of photon energy. Photoelectrons were measured at a normal emission angle.

Fig. 5 Integrated intensity from CO ($1\pi + 5\sigma$) and CO 4σ adsorbate MO levels as a function of photon energy for a 45° electron take-off angle. The right hand panel shows the ratio similarly to Fig. 4.

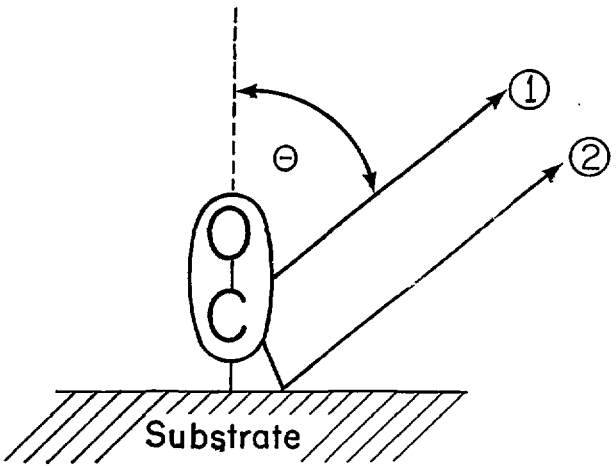

Fig. 1 XBL 7611-4377

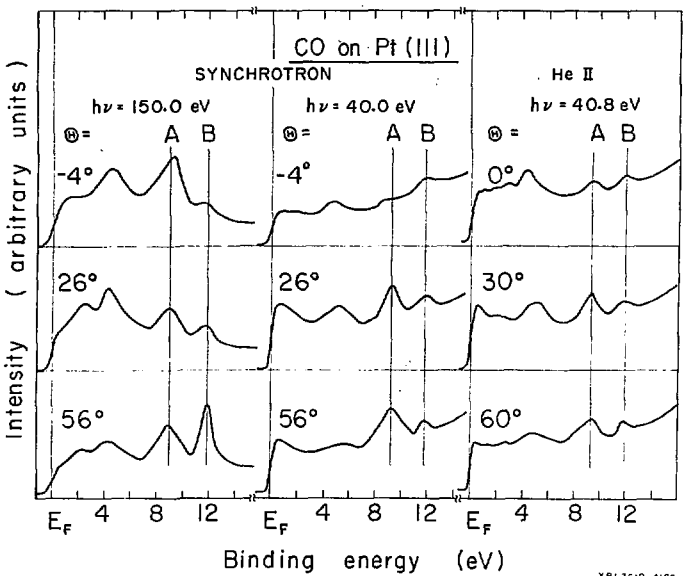
CO on Pt (111)
SYNCHROTRON
He II
hν = 150.0 eV
hν = 40.0 eV
hν = 40.8 eV
Θ =
A
B
-4°
26°
56°
0°
30°
60°
Intensity (arbitrary units)
E_F
4
8
12
Binding energy (eV)
XBL7610-4180

Fig. 2

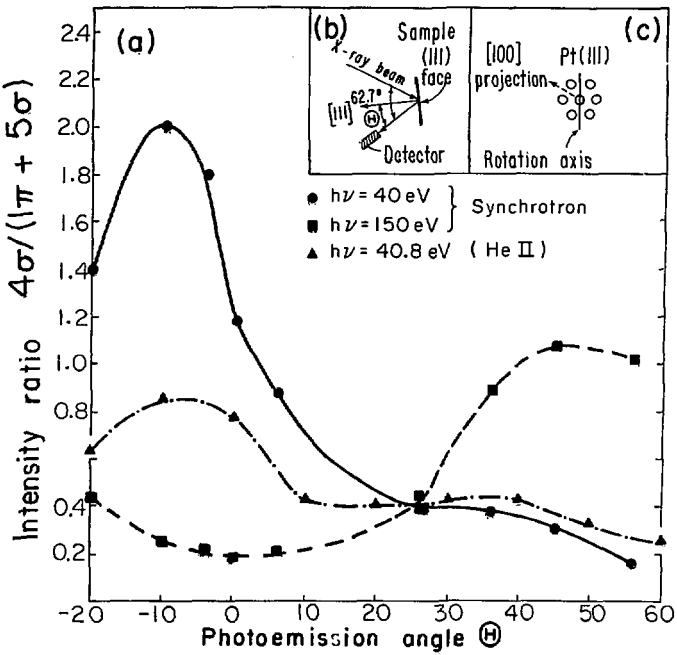

Fig. 3

XBL769-4026

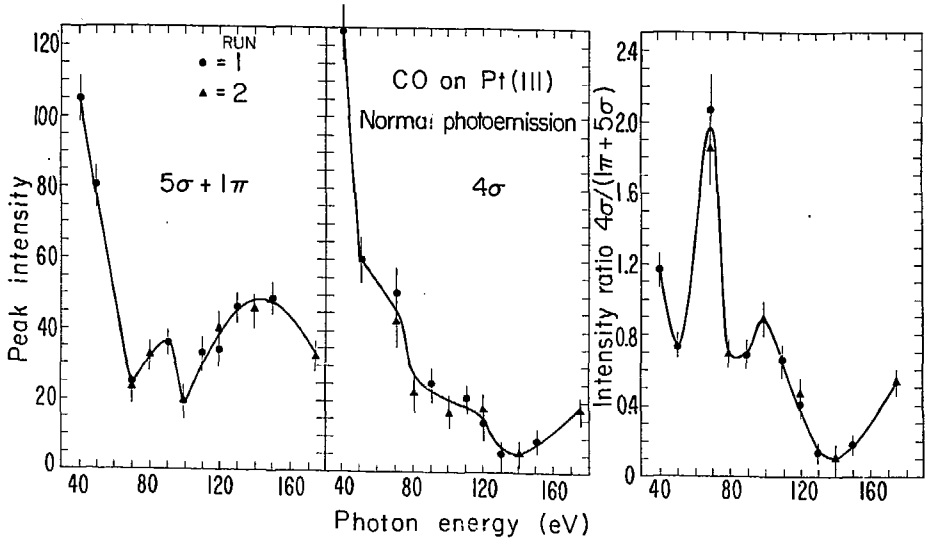

XBL773-696

Fig. 4

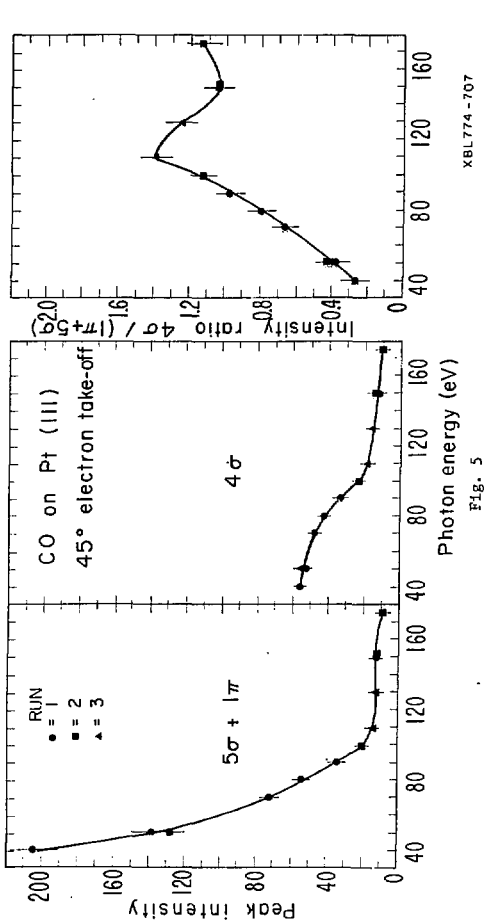
Peak intensity
RUN
● = 1
■ = 2
▲ = 3
5σ + 1π
CO on Pt (111)
45° electron take-off
4σ
Intensity ratio 4σ / (1π+5σ)
Photon energy (eV)
XBL774-707

Fig. 5

SUMMARY

In this thesis I have attempted to present experimental work in photoemission from solids and adsorbates which has made pratical utilization of a substantial region of the electromagnetic energy spectrum, from ∿30 eV(413Å) to ∿300 eV(41Å). Photoelectron spectroscopy, over the last decade, has become a technique of choice to study the total electronic valence-band density of states in solids; however, until the advent of a suitable variable-energy photon source such as synchrotron radiation the technique had been severely inhibited. With access to the synchrotron radiation available at SSRL the last two years, we have been able to perform several novel experiments.

A summation of our main research goals, as exemplified in the previous chapters, has to focus around an interest to assess the feasibility and value of photoemission experiments at photon energies between 30 eV and several hundred eV. Several questions which we asked originally have now been answered: is there an advantage to studying clean surfaces and adsorbate-substrate systems using variable photon energies, particularly above 100 eV, and what is the nature of cross-section modulations in this energy region? The result has been that photoemission experiments in the range 50-250 eV reveal several new phenomena which are not observed in conventional ultraviolet ($\hbar\omega < 50$ eV) or x-ray ($\hbar\omega \sim 1$ keV) photoelectron spectroscopy.

Photoemission spectra which are obtained by exciting valence electrons in solids have revealed strong attenuations in the photoionization cross-section over a small energy range, for initial state wavefunctions

having at least one radial node. Such effects, which we have observed for Ag(4d), Au(5d), and Pt(5d) valence bands, are attributed to and explained in terms of a "Cooper minimum". For 3d initial state wavefunctions which possess no radial nodes, the effect is absent. Our studies with a monolayer of CO adsorbed on Pt demonstrate that future adsorbate studies can benefit from synchrotron experiments at high photon energies where there is selectivity for reducing substrate intensity due to "Cooper minima". A corollary finding is that qualitative predictions of adsorbate intensities can be formulated from theoretical cross-sections of gas phase molecules and experimentally determined substrate valence band photoemission intensities. Synchrotron radiation has also allowed us to obtain unique information about surface electronic structure, via photoemission with photons of high enough energy to create ionized electrons with the kinetic energy to have minimum electron mean free paths. Beyond this, the developing technique of angle-resolved photoemission has been utilized to yield the angular distribution of photoelectrons in each orbital peak of an adsorbate and thusly to map out the orientation of the orbitals, hence the adsorbate. The final sections of the thesis have been included to preview future directions toward which photoemission experiments are aimed, namely the determination of adsorption sites and the nature of the bonding of a chemisorbed atom or molecule.

ACKNOWLEDGEMENTS

The completion of my graduate work at Berkeley has been made possible by the help of a great many people to whom I am sincerely grateful. It is with particular pleasure that I thank Professor David A. Shirley for many contributions and the encouragement which he has shown throughout my research. I have also benefited in large part from early associations and discussions with Dr. Jack Hollander, Dr. Tihomir Novakov, Dr. H. F. Schaefer, and Dr. Gunter Kaindl. Certainly of no less importance has been the contribution from my colleagues in the electron spectroscopy research group at Berkeley. I am particularly indebted to Dr. Joachim Stöhr, Dr. Steven Kowalczyk, Dr. Read McFeely, Paul Wehner, R. Stanley Williams, and Dr. Gary Schwartz for their many contributions over the years. I have had the pleasure of working with and learning from Dr. Lothar Ley, Dr. Shuit-Tong Lee, Dr. Şefik Süzer, Dr. Richard Martin, Dr. Bernice Mills, Dr. Richard Streater, Dick Rosenberg, Mike White, Erwin Poliakoff, Ken Mills, and Dennis Trevor. I would also like to acknowledge the technical support people who have been invaluable; Mr. D. N. Voronin, Mr. Gene Miner, Mr. Joseph Katz, Mr. Dick Escobales, and Mr. Richard Strudwick. I wish to thank Dr. R. Z. Bachrach and the Xerox Group for their assistance during the initial phase of our synchrotron radiation work. For last I have saved my special thanks for Mrs. Winifred Heppler and Mrs. Karen Janes.

(This work was done with support from the U.S. Energy Research and Development Administration.)